R-11-17

Hydraulic effects of unsealed boreholes

Numerical groundwater flow modelling of the Forsmark and Laxemar sites

Niclas Bockgård, Golder Associates AB

June 2011

Svensk Kärnbränslehantering AB
Swedish Nuclear Fuel
and Waste Management Co

Box 250, SE-101 24 Stockholm
Phone +46 8 459 84 00

ISSN 1402-3091
SKB R-11-17
ID 1240444

Hydraulic effects of unsealed boreholes

Numerical groundwater flow modelling of the Forsmark and Laxemar sites

Niclas Bockgård, Golder Associates AB

June 2011

Summary

The objective of the work was to investigate hydraulic effects of open and poorly sealed boreholes on groundwater flow conditions through simulations using a numerical groundwater model. Specifically, the boreholes KFM07A, KFM09A, and KFM09B in Forsmark and the boreholes KLX04, KLX06, and KLX10 in Laxemar were studied. The criteria for the selection of these boreholes were that the boreholes should represent typical conditions of the site, the borehole length should exceed 500 m, and that several major fractured zones should be intersected. The boreholes KFM07A and KLX06, respectively, were selected as reference boreholes for more detailed studies of different sealing schemes.

The model setup of the Forsmark model followed the Forsmark 2.2 regional-scale conceptual hydrogeological model. The model domain was approximately 15 km (north–south) × 10 km (west–east) ×1.2 km (depth). The 131 deformation zones and three layers of superficial horizontal sheet joint were modelled deterministically. A stochastic discrete fracture network (DFN) representing fractures and minor deformation zones were also generated between the deterministic deformation zones inside central model volume. The side lengths of the square fractures were from 1,000 m down to 10 m. In order to resolve the details of flow in to and out from the borehole, a more detailed DFN was generated in a zone around the borehole KFM07A, where fractures down to a side length of 0.5 m were considered.

The model setup of the Laxemar model followed the SDM-Site Laxemar (Laxemar 2.3) regional-scale conceptual hydrogeological model. The model domain was approximately 12 km (north–south) × 20 km (west–east) × 2.1 km (depth). A number of 71 deformation zones were modelled deterministically, and one realization of a stochastic DFN, the so-called hydrogeological DFN model base case, was imported to the model. Similar to the Forsmark case, a more detailed DFN was also generated around the reference borehole KLX06.

The numerical groundwater modelling code DarcyTools was used for the simulations. Continuum hydraulic property fields for the flow simulations were generated from the deterministic deformation zones and the modelled DFN. DarcyTools has a special routine for simulation of open boreholes. A reference borehole plugging scheme and a simplified version were applied for the reference boreholes. The concept for borehole sealing included alternating sections of silica-concrete and bentonite along the borehole. In the models, appropriate values of hydraulic conductivity were assigned to the grid cells representing the studied boreholes to accommodate simulation of the borehole sealing.

The hydraulic impacts on the groundwater flow conditions of the open (unsealed) and poorly sealed boreholes were investigated by steady-state simulations. No salinity and no density effects were included in the simulations. The variables that were investigated were changes in the hydraulic head and flow fields around the boreholes at repository depth, the total flow through a defined rock volume surrounding the boreholes, and the flow along the boreholes. Also, in order to study the impact on advective travel time for water and solutes between repository depth and surface, particle tracking was performed between a horizontal plane at –600 m and the –50 m level.

The simulations indicated that the open boreholes have a considerable hydraulic influence, especially on hydraulic heads at large depths. There was a difference in the hydraulic function of the open boreholes when comparing the two sites studied for the present-day hydraulic boundary conditions. In Forsmark, as a discharge area for deeper groundwater, open boreholes acted as easy path ways for groundwater from repository depth to surface. In Laxemar, on the other hand, being in part a recharge area for deeper groundwater, open boreholes acted as paths from surface to depth. The open boreholes increased the groundwater turnover in the borehole site rock volume with about 17% in the Forsmark model, but the effect on the groundwater turnover in the Laxemar model was small. This difference is due to the much lower permeability at repository depth in Forsmark compared to Laxemar, which makes the effect of the open boreholes more apparent in Forsmark. The different influence on groundwater flow is also reflected in the influence on solute transport in the surrounding bedrock, where the open boreholes had a strong influence in the Forsmark model but not in the Laxemar model. This is shown by the influence on the distributions of advective travel times and path lengths for particles.

The simulations with sealed boreholes (reference and simplified plugs) indicated that the larger-scale hydraulic influences of sealed boreholes are insignificant. This is as expected since the conductance of even the degrades silica-concrete sections of the plugged borehole is very small compared to high transmissive fractures. However, the flow along the concrete-plug sections was significantly above the natural flow in the surrounding rock, even though it did not influence the overall hydraulic head or flow fields. The reason for this is that the hydraulic conductivity of the degraded silica concrete generally is higher than the hydraulic conductivity of the rock. A conclusion is therefore that the positions of the bentonite sections in relation to conductive structures are important.

Sammanfattning

I ett projekt om borrhålsförslutning har Svensk Kärnbränslehantering AB (SKB) utvecklat tekniker för förslutning av undersökningsborrhål. Den valda principen för förslutningen är att täta sektioner av borrhålet med låg sprickfrekvens och transmissivitet med t ex bentonit och att fylla sektioner som genomkorsas av transmissiva sprickor eller deformationszoner med ett fysiskt stabilt material som inte behöver ha särskilt låg genomsläpplighet, t ex kvartscement.

Syftet med föreliggande arbete var att undersöka påverkan på grundvattenströmningen från öppna och tätade undersökningsborrhål genom simuleringar med en numerisk grundvattenmodell. Mer specifikt studerades borrhålen KFM07A, KFM09A och KFM09B i Forsmark och KLX04, KLX06 och KLX10 i Laxemar. Kriterierna för valet av dessa borrhål var att borrhålen skulle vara representativa för de generella förhållandena på respektive plats, att borrhålen skulle vara minst 500 m långa och att flera betydande sprickzoner skulle genomkorsas. Borrhålen KFM07A och KLX06 valdes ut som referensborrhål för mer detaljerade studier av olika utformningen av borrhålstätningen.

Modelluppsättningen för Forsmark följde den regionala hydrogeologiska konceptuella modellen Forsmark version 2.2. Modelldomänens utsträckning var ungefär 15 km (nord–syd) × 10 km (väst–öst) × 1,2 km (i djupled). De 131 deformationszonerna och de tre skikten med ytliga horisontella bankningsplan modellerades deterministiskt. En realisering av ett stokastiskt diskret spricknätverk (DFN), som representerade enskilda sprickor och mindre deformationszoner, genererades också mellan de deterministiska deformationszonerna i den centrala delen av modellvolymen. Kvadratiska sprickor med en sidlängd från 1 000 m ned till 10 m genererades. För att kunna beskriva detaljer i strömningen in och ut ur borrhålet skapades även ett mer detaljerat spricknätverk i en zon runt borrhål KFM07A, där sprickor med en sidlängd ned till 0,5 m inkluderades.

Modelluppsättningen för Laxemar följde den regionala hydrogeologiska konceptuella modellen SDM-Site Laxemar (Laxemar 2.3). Modelldomänens utsträckning var ungefär 12 km (nord–syd) × 20 km (väst–öst) × 2,1 km (i djupled). De 71 deformationszonerna modellerades deterministiskt, och en realisering av ett stokastiskt diskret spricknätverk (det så kallade ”hydrogeological DFN model base case”) importerades till modellen. På samma sätt som för Forsmarksmodellen skapades också ett mer detaljerat spricknätverk runt referensborrhålet KLX06.

Grundvattenmodelleringsverktyget DarcyTools användes för simuleringarna. Ett hydrauliskt konduktivitetsfält genererades utifrån egenskaperna hos de deterministiska deformationszonerna och det diskreta spricknätverket. I DarcyTools finns särskilda funktioner för simulering av öppna borrhål. En referensutformning för borrhålstätningen och en förenklad variant implementerades i modellen för de två referensborrhålen. Det studerade konceptet för borrhålstätning består av omväxlande sektioner med kvartscement och bentonit längs med borrhålet. Borrhålstätningen simulerades i de numeriska modellerna genom att ansätta den hydrauliska konduktivitet som motsvarar respektive material till de gridceller som representerade borrhålen.

Påverkan på grundvattenströmningen från de öppna (otätade) och tätade borrhålen studerades genom steady-state-simuleringar. Salinitet och densitetseffekter inkluderades inte i modellen. Variablerna som studerades var grundvattnets totalpotential och flödet runt borrhålen på förvarsdjup, det totala flödet genom en definierad bergvolym runt borrhålen samt flödet längs med borrhålen. För att studera påverkan på den advektiva transporttiden för vatten och lösta ämnen mellan förvarsdjup och markytan gjordes partikelspårning mellan nivån –600 m och nivån –50 m i den numeriska modellen.

Resultaten från simuleringarna indikerade att de öppna borrhålen hade en betydande hydraulisk påverkan på grundvattnets på stort djup. Vid en jämförelse uppvisade de två studerade platserna en skillnad i den hydrauliska funktionen hos öppna borrhål under dagens hydrauliska randvillkor. I Forsmark, som bedöms vara ett utströmningsområde för djupare grundvatten, fungerar de öppna borrhålen som flödesvägar för grundvattnet från förvarsdjup upp till markytan. I Laxemar, som å andra sidan delvis är ett inströmningsområde för grundvatten från ytan mot djupet, fungerar de öppna borrhålen som flödesvägar från markytan mot djupet. De öppna borrhålen orsakade en ökning av det totala grundvattenflödet i bergvolymen runt borrhålen med omkring 17 % i Forsmarksfallet, men effekten på det totala grundvattenflödet var liten i Laxemarmodellen. Denna skillnad förklaras

av den mycket lägre permeabiliteten på förvarsdjup i Forsmark jämfört med Laxemar, vilket gör effekten av öppna borrhål mer uttalad i Forsmark. Skillnaden ses också i påverkan på ämnestransporten i det omgivande berget, där de öppna borrhålen hade en stor påverkan i Forsmarksmodellen men inte i Laxemarmodellen. Detta uttrycks i påverkan på fördelningarna för advektiv transporttid och transporterad sträcka för de spårade partiklarna.

Simuleringarna med tätade borrhål (både referensutformning och förenklad utformning) indikerade att påverkan av de tätade borrhålen är obetydlig sett i större skala. Den förenklade borrhålstätningen hade i stort sett lika bra funktion som referensutformningen. Det var som förväntat eftersom konduktansen hos även en urlakad kvartscementsektion i ett pluggat borrhål är mycket låg jämfört med den hos högtransmissiva sprickor och sprickzoner. Flödet längs med borrhålet i kvartscementsektionerna var dock betydligt högre än det naturliga flödet i omgivande berg, även om det inte påverkade grundvattnets totalpotential eller flöde i större rumslig skala. Orsaken till detta är att den hydrauliska konduktiviteten i en urlakad kvartscementplugg generellt sett är högre än det omgivande bergets hydrauliska konduktivitet. En slutsats är därför att placeringen av de täta bentonitsektionerna i förhållande till de permeabla strukturer som skär borrhålet är betydelsefull.

Contents

1 Introduction

1.1 Background

In the project Sealing of boreholes SKB (Swedish Nuclear Fuel and Waste Management Co) develops techniques for sealing of investigation boreholes. The basic principle chosen for borehole sealing is to tightly seal sections of the borehole with low fracture frequency and low transmissivity (with e.g., bentonite), and to fill the sections of the borehole that are intersected by transmissive fractures or deformation zones with physically stable material that does not need to be very tight (e.g., with silica concrete) (Pusch et al. 2011). One of the goals of the project is to develop borehole sealing strategies for a number of reference investigation boreholes at the two site investigation areas Forsmark and Laxemar (Pusch et al. 2011). The overall aim of this study is to quantify the hydraulic performance of poorly sealed boreholes in the vicinity of a final repository for spent nuclear fuel.

1.2 Objectives

The objective of the work reported in this report was to investigate hydraulic effects of poorly sealed boreholes through simulations using numerical groundwater models. Specifically, the effects of the three boreholes KFM07A, KFM09A, and KFM09B in the Forsmark site investigation area and the three boreholes KLX04, KLX06, and KLX10 in the Laxemar site investigation area were studied.

The specific objectives were to study the differences in hydraulic head and flow fields at repository depth and differences in flow paths and advective travel times between repository depth and the surface for three different cases:

1. Model without boreholes. Bedrock only.
2. All boreholes open.
3. One borehole (KFM07A and KLX06, respectively) sealed with a degraded plug and the other two removed (bedrock only).

The borehole plug design and the character of the degraded plug are explained in Section 2.1.6.

No repository tunnels or any specific repository layouts were included in the models. The effect on groundwater flow and performance measures of the presence of open boreholes close to the intended final repository in Forsmark has been assessed within the SR-Site project (Joyce et al. 2010). In that study also the repository structures were included and the particle tracking was started at approved canister positions.

2 Hydrogeological models

2.1 Hydrogeological model of the Forsmark site

The hydrogeological conceptual model applied in this study was the Forsmark 2.2 regional-scale hydrogeological model (described in Follin et al. 2007). If not stated otherwise, the model concepts and properties used were imported from a preliminary version (dated June 2008) of the model reported in Svensson and Follin (2010).

2.1.1 Model domain and hydrologic boundaries

The dimensions of the model volume were approximately 15 km (north–south), 10 km (west–east), and 1.2 km (vertical) (Figure 2-2). The horizontal coverage of the model domain was thus roughly equal to the Forsmark 2.2 general regional-scale model domain, but the vertical coverage of the hydrogeological model volume was smaller (Follin et al. 2007) compared to the general model volume, which has its bottom at the elevation –2,100 m (RHB 70). The boundary of the model domain follows the topographical water divide in the southwest, and in the north and the south it is oriented essentially parallel to the topographic gradient. The boundary to the northeast lies at a major bathymetric break at the sea floor (SKB 2008), and is located sufficiently far away from the shoreline that it does not influence the groundwater flow in the model area for the present location ofthe shoreline.

A local coordinate system for the Forsmark model was used in this study, where (X (E), Y (N)) = (0, 0) in the local system corresponds to (1626000, 6692000) in the Swedish national RT 90 2.5 gon W system. The Z-coordinate (elevation) is given in the national RHB 70 levelling system.

2.1.2 Near-surface hydrology

The groundwater recharge applied in this study for Forsmark was 130 mm/yr. This can be compared to the mean annual runoff according to the final site description of Forsmark (SKB 2008), which was 150 mm/yr.

A soil cover was not explicitly modelled. Instead a more permeable and porous surface layer was modelled to a depth of 20 m below the surface (land or sea bottom). In this layer a constant vertical hydraulic conductivity of $1 \cdot 10^{-6}$ m/s was applied, whereas an exponential depth decrease was used for the horizontal hydraulic conductivity:

$$K = 5 \cdot 10^{-3}\ 10^{-d/(3\ \mathrm{m})}\ \mathrm{m/s} \quad (d \leq 20\ \mathrm{m}) \qquad (2\text{-}1)$$

where d is the depth below surface, with the constraint $K \geq 1 \cdot 10^{-6}$ m/s (Figure 2-1 (a)). A similar relation was used for the kinematic porosity n (Figure 2-1 (b)):

$$n = 5 \cdot 10^{-2}\ 10^{-d/(20\ \mathrm{m})} \quad (d \leq 20\ \mathrm{m}) \qquad (2\text{-}2)$$

The applied network of streams (grid cells with high hydraulic conductivity) that were imported from Svensson and Follin (2010) is shown in Figure 2-3.

2.1.3 Deformation zones and sheet joints

A total of 131 deterministic deformation zones have been modelled for Forsmark (Figure 2-4) (Stephens et al. 2007). The hydraulic parameterisation of the deformation zones in the Forsmark 2.2 model stage is described in Follin et al. (2007). The zones were modelled as homogeneous in the lateral direction but with a strong depth dependence in the hydraulic properties in the vertical direction.

In addition to the deformation zones, the model also contained deterministic structures representing the superficially located horizontal sheet joints that are characteristic for the Forsmark area (Follin et al. 2007). These were represented as three 1m thick layers running parallel to the ground surface at approximately 30, 70, and 110 m below the surface (Figure 2-5).

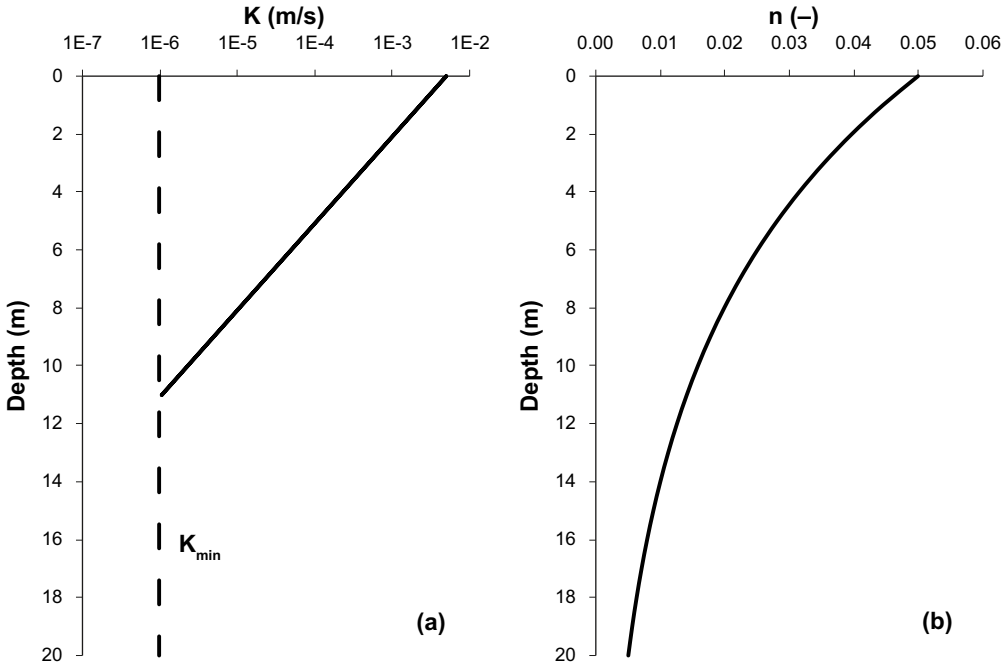

Figure 2-1. *Modelled depth dependence of (a) hydraulic conductivity and (b) kinematic porosity in the surface layer down to 20 m below surface.*

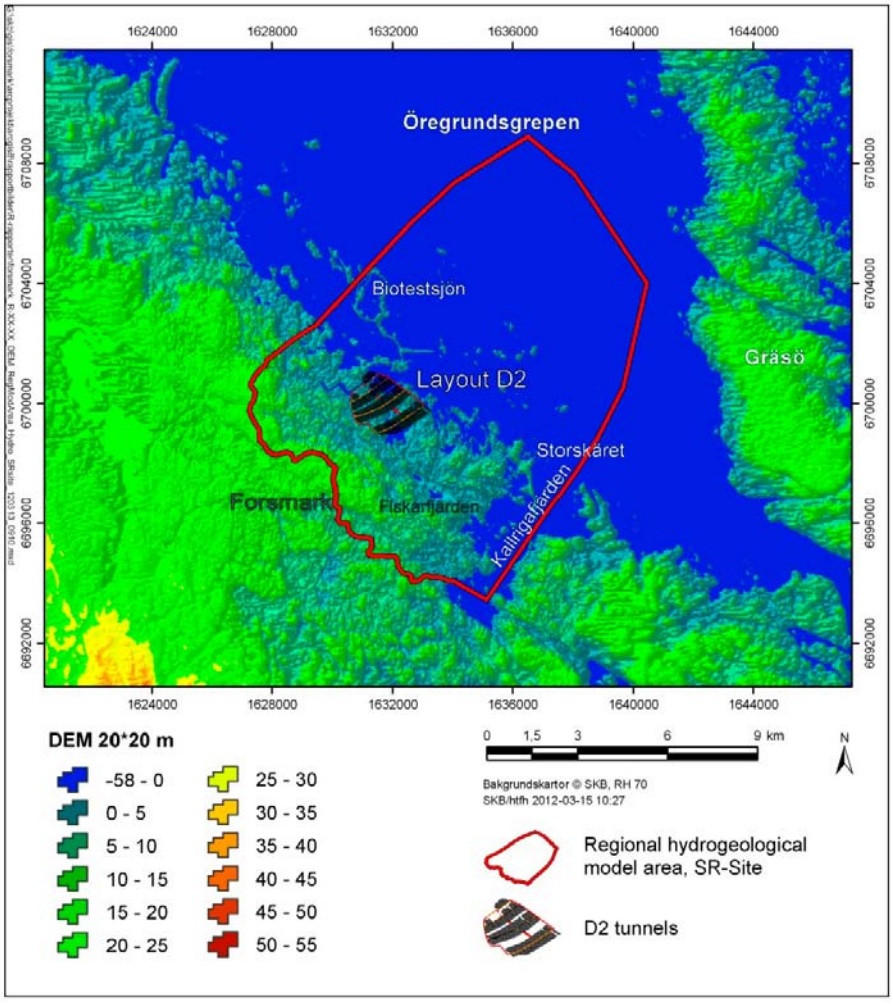

Figure 2-2. *Topographical map of the Forsmark area. The model domain is shown by a red line.*

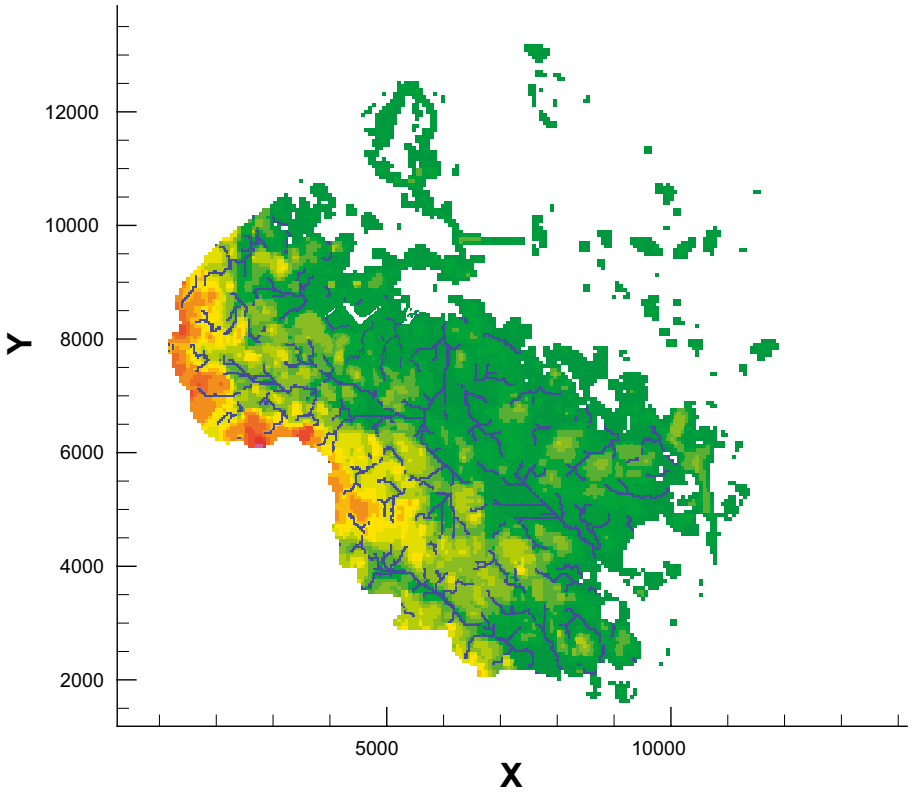

Figure 2-3. *The applied network of streams (blue) from Svensson and Follin (2010) on a background topographical map.*

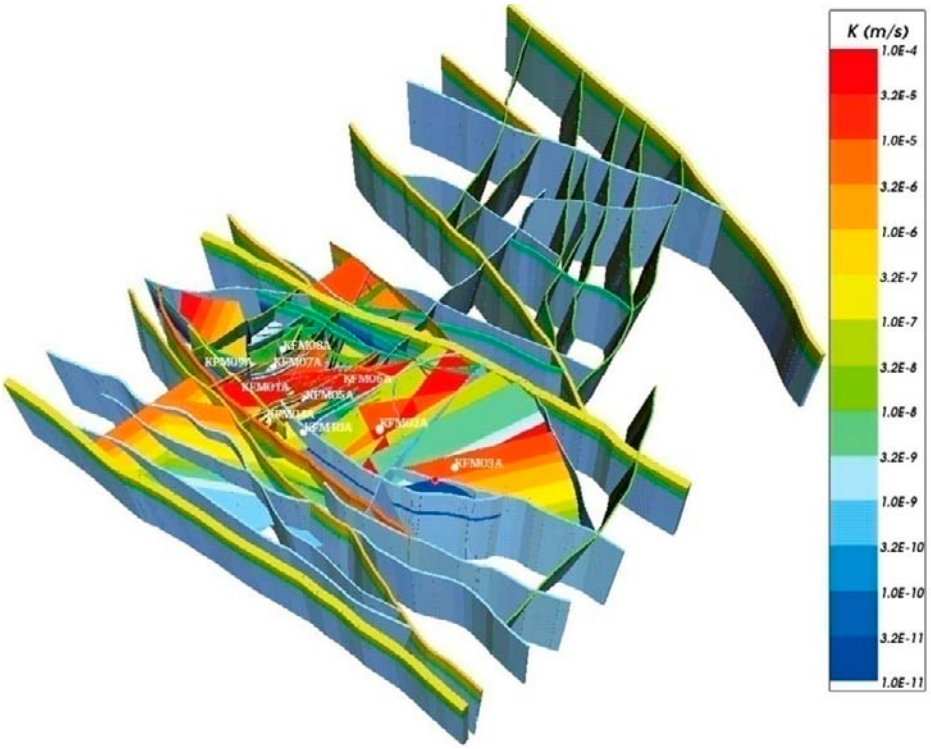

Figure 2-4. *Deformation zone model for Forsmark. The zones are coloured by the hydraulic conductivity within the zones and are drawn with their defined hydraulic thickness. (Reproduced from SKB 2008.)*

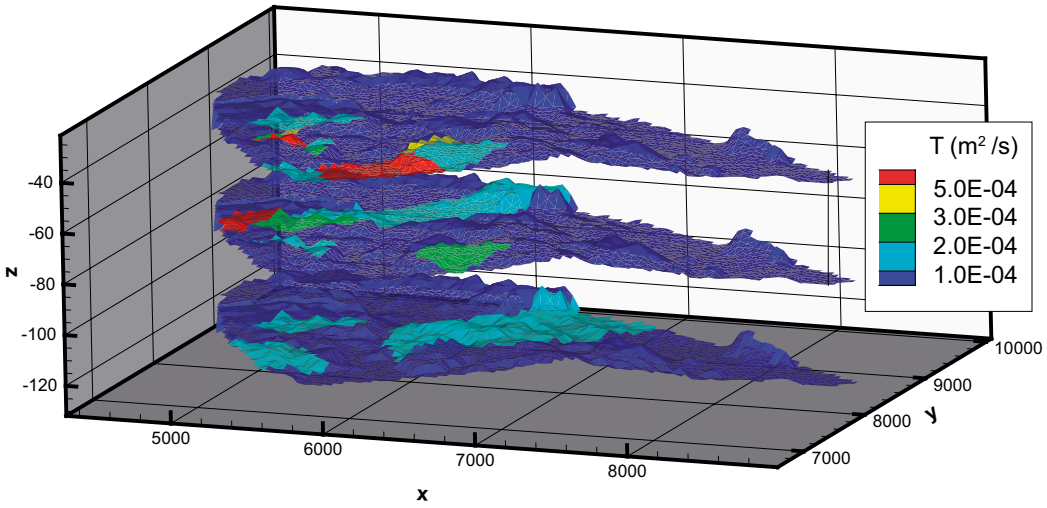

Figure 2-5. *The three generalised sheet joint structures at approximately 30, 70, and 110 m below ground surface that represent the sheet joints.*

2.1.4 Fracture domains

A stochastic discrete fracture network representing fractures and minor deformation zones (hydro-geological DFN) was modelled inside the so called fracture domains. Of the six fracture domains, domains FFM01–03 and FFM06 occur in the target volume for the repository (Figure 2-6), whereas FFM04–05 are located in the bordering bedrock southwest and northeast of the target volume, respectively. The DFN statistical properties and hydraulic properties were equal for FFM01 and FFM06 (group 1), and for FFM03, FFM04, and FFM05 (group 2). Each fracture domain group was subdivided into depth intervals. Five fracture sets were modelled for each fracture domain group and depth interval (Appendix 2). The DFN parameter values used were preliminary values for the Forsmark 2.2 modelling stage, and hence do not correspond exactly to the final version reported in Follin et al. (2007).

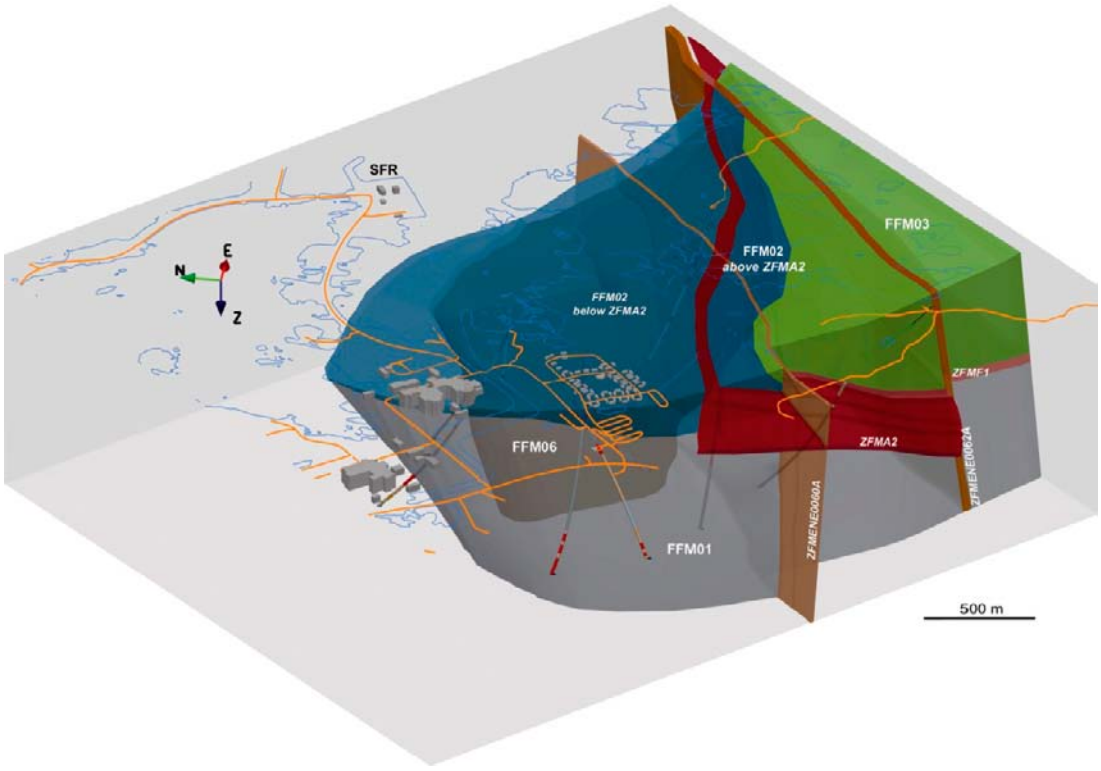

Figure 2-6. *Perspective view of the three-dimensional representation of the fracture domains FFM01, FFM02, FFM03, and FFM06 (reproduced from Olofsson et al. 2007).*

All stochastic fractures were assigned a geometrical thickness of 0.1 m and a transmissivity according to a semi-correlated transmissivity distribution, i.e., the transmissivity was correlated to the fracture size, but not perfectly. In DarcyTools the transmissivity (m^2/s) of the stochastic fractures follows a log-uniform distribution about a power-law correlated mean according to:

$$log\ T = log\left[a \left(\frac{l}{100\ \mathrm{m}} \right)^b \right] + d\ U \qquad (2\text{-}3)$$

where l is the side length of the square fracture, a, b, and d are constants and U is a stochastic variable with a uniform distribution in the interval (–0.5, 0.5) (Svensson and Ferry 2010). This is slightly different to the semi-correlated distribution recommended in Follin et al. (2007), which have a log-normal distribution about the size-correlated mean transmissivity. All fracture sets within one fracture domain and depth interval shared the same transmissivity distribution (Table 2-1). One realization of the stochastic DFN was applied in this study, see Section 4.3.3.

Outside the fracture domains a minimum hydraulic conductivity of $1 \cdot 10^{-7}$ m/s was applied in the upper 200 m below the ground surface, $1 \cdot 10^{-8}$ m/s in the depth interval 200–400 m below the ground surface, and $3 \cdot 10^{-9}$ m/s below 400 m.

Table 2-1. Constants of the transmissivity distribution (Equation 2-3) for the fracture domains in Forsmark (elevations in RHB 70) (Values from the applied preliminary version of the model reported in Svensson and Follin (2010).)

Fracture domain	a	b	d
FFM01, 06 above –200 m	$1.18 \cdot 10^{-6}$	1.3	2.0
FFM01, 06 below –200 m, above –400 m	$9.70 \cdot 10^{-9}$	0.5	2.0
FFM01, 06 below –400 m	$3.97 \cdot 10^{-10}$	0.5	2.0
FFM02	$1.51 \cdot 10^{-7}$	0.7	2.0
FFM03, 04, 05, above –400 m	$6.50 \cdot 10^{-8}$	0.4	1.6
FFM03, 04, 05, below –400 m	$6.02 \cdot 10^{-8}$	0.3	1.0

2.1.5 Transport properties

Only advective transport was considered in this study. The only transport parameter needed is then the kinematic (or transport) porosity. The kinematic porosity was derived from the porosity of the underlying deformation zone model and the DFN. The porosity of the deformation zones was in SDM Forsmark estimated from the transmissivity of the zones through an empirical relation (Follin et al. 2008). The kinematic porosity of the fractures of the DFN was set to 10^{-3} (over the thickness of 0.1 m). Further, the lowest porosity allowed was 10^{-5}. This porosity was also assumed outside the deformation zones and the fracture domains following (Follin et al. 2007).

2.1.6 Boreholes

Candidate boreholes

The three core drilled investigation boreholes KFM07A, KFM09A, and KFM09B in the Forsmark site investigation area (Figure 2-7) were selected as candidate boreholes for the virtual borehole sealing study (Pusch et al. 2011). The criteria for the selection of these boreholes were that the boreholes should represent typical conditions of the site, the borehole length should exceed 500 m, and that several major deterministic deformation zones should be intersected. Of these three boreholes, KFM07A was selected as a reference borehole for more detailed studies of the borehole sealing scheme. This decision was based on two main criteria (Pusch et al. 2011):

1. The importance of the borehole with respect to its hydraulic function. A borehole that intersects a few high-transmissive zones in a relatively unfractured background rock may be more important regarding hydraulic short-circuiting than a borehole through more intensely fractured rock.
2. The difficulties in performing the borehole sealing operation. The criterion 1) implies that there may be a higher hydraulic gradient across the plug in a borehole that intersects few hydraulic active zones. This will increase the risk of piping and erosion.

The motivation to include also the other two boreholes was to simulate and investigate the simultaneous effect on the groundwater flow of a number of open boreholes in the area. A detail picture of the modelled deformation zones that intersect the boreholes is shown in Figure 2-8. The only borehole intersected by the sheet joins (Section 2.1.3 is KFM07A).

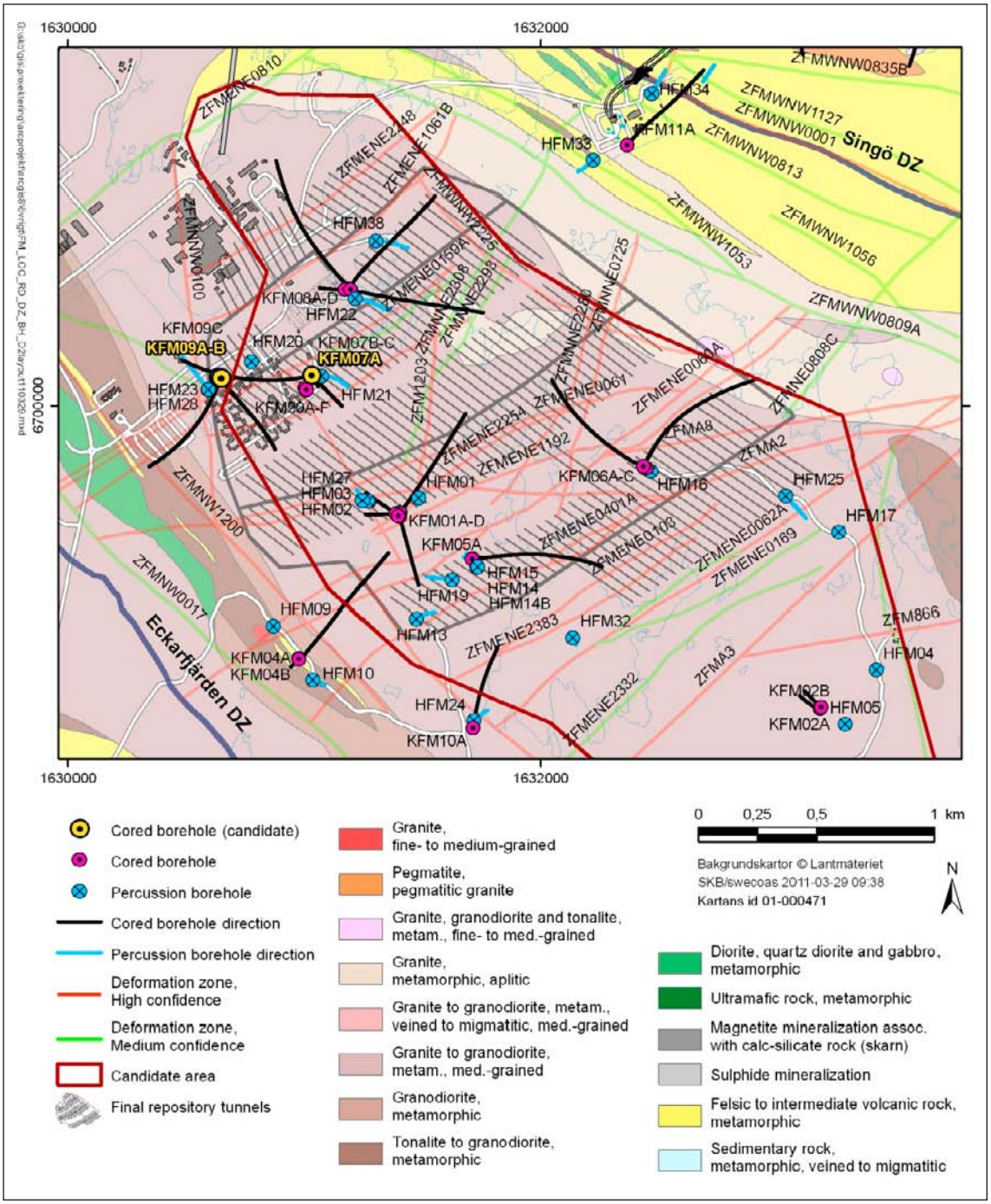

Figure 2-7. *Geology of the Forsmark area and location of the studied (candidate) boreholes in relation to the proposed layout of the final repository (Layout D2).*

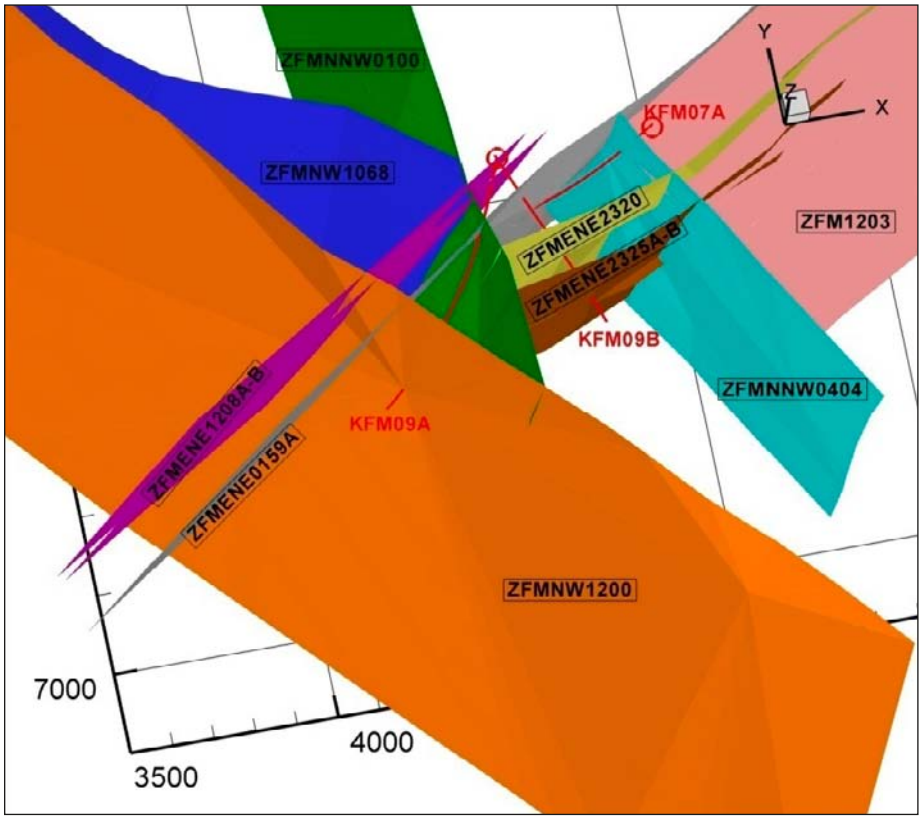

Figure 2-8. *Deformation zones crossing the boreholes. The horizontal sheet joint are left out from the figure.*

Borehole plugs

The borehole sealing concept is described in Pusch et al. (2011). The basic principle is to seal the borehole with tight bentonite plugs in the sections of the borehole where the surrounding rock is low-permeable and with physically stable silica-concrete plugs where the borehole intersects water-bearing fracture zones. The granular sand skeleton of the silica-concrete plug sections is resistant to chemical dissolution and it will keep the bentonite sections in place and protect them from deformation and erosion. In this study the intension was to study the hydraulic behaviour of a degraded plug (Table 2-2). The hydraulic conductivity should represent that of silica concrete where the cement has dissolved and that of low density bentonite, respectively (Pusch R 2008, personal communication). A borehole plugging scheme for the reference borehole KFM07A was developed in two versions: A reference plug and a simplified version (Figure 2-9).

Table 2-2. Properties for materials in the degraded borehole plug.

Material	Hydraulic conductivity (m/s)
Silica concrete	$1 \cdot 10^{-6}$
Bentonite	$1 \cdot 10^{-8}$

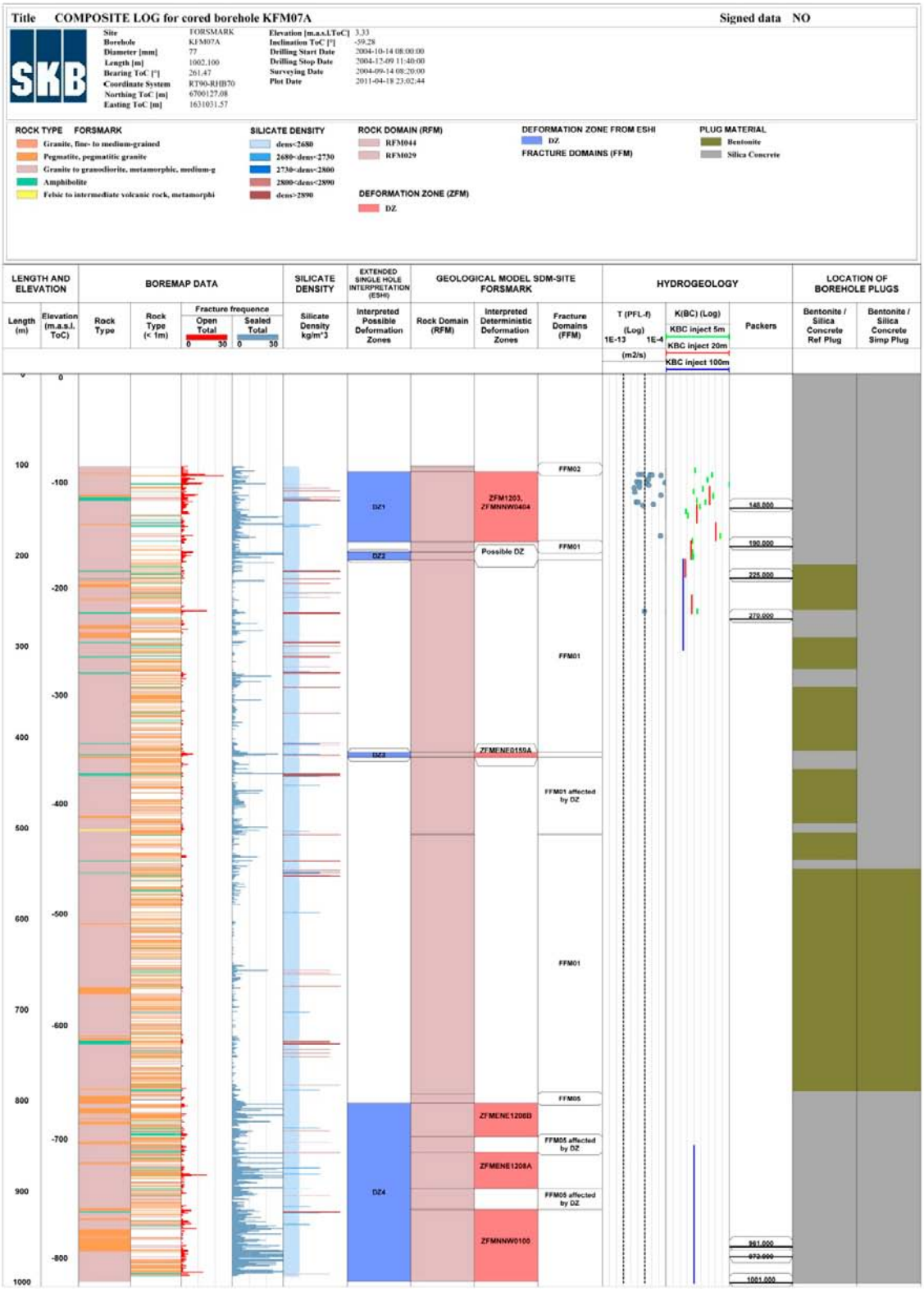

Figure 2-9. *Composite geological and hydrogeological log for borehole KFM07A together with the proposed location (Pusch et al. 2011) of borehole plugs. (Ref Plug = reference plug, Simp Plug = simplified plug.)*

2.2 Hydrogeological model of the Laxemar site

The hydrogeological conceptual model of Laxemar applied in this study was the SDM-Site Laxemar regional-scale hydrogeological model (SKB 2009a). If not stated otherwise the concepts and properties were imported from a preliminary version (dated May 2009) of the model reported in Svensson and Rhén (2010).

2.2.1 Model domain and hydrologic boundaries

The dimensions of the model volume were approximately 12 km (north–south), 20 km (west–east), and 2.1 km (vertical) (Figure 2-10), roughly equal to the SDM-Site Laxemar regional-scale model domain. The boundary of the model domain follows the topographical water divide in the north and the west, and in the south it is oriented essentially parallel to the topographic gradient. The boundary to the east is located in the strait of Kalmarsund, and it is sufficiently far away from the shoreline that it is judged to not influence the groundwater flow in the model area for the present location of the shoreline (SKB 2009a). A local coordinate system for the Laxemar model was used in this study, where (X (E), Y (N)) = (0, 0) in the local system corresponds to (1539000, 6360000) in the Swedish national RT 90 2.5 gon W system. The Z-coordinate (elevation) is given in the national RHB 70 levelling system.

2.2.2 Near-surface hydrology

The groundwater recharge applied in this study for Laxemar was 165 mm/yr. This is in agreement with the estimated mean annual runoff according to the SDM-Site Laxemar site description (SKB 2009a), which was 160–170 mm/yr.

The soil layer and the surficial bedrock was modelled as a more permeable and porous surface layer in the same way as for the Forsmark model (Section 2.1.2). The same exponential depth decrease functions for horizontal hydraulic conductivity and kinematic porosity as for Forsmark were applied, whereas the constant vertical hydraulic conductivity was set to $5 \cdot 10^{-6}$ m/s in the surface layer in this case. The defined network of streams (Svensson and Rhén 2010) is shown in Figure 2-10.

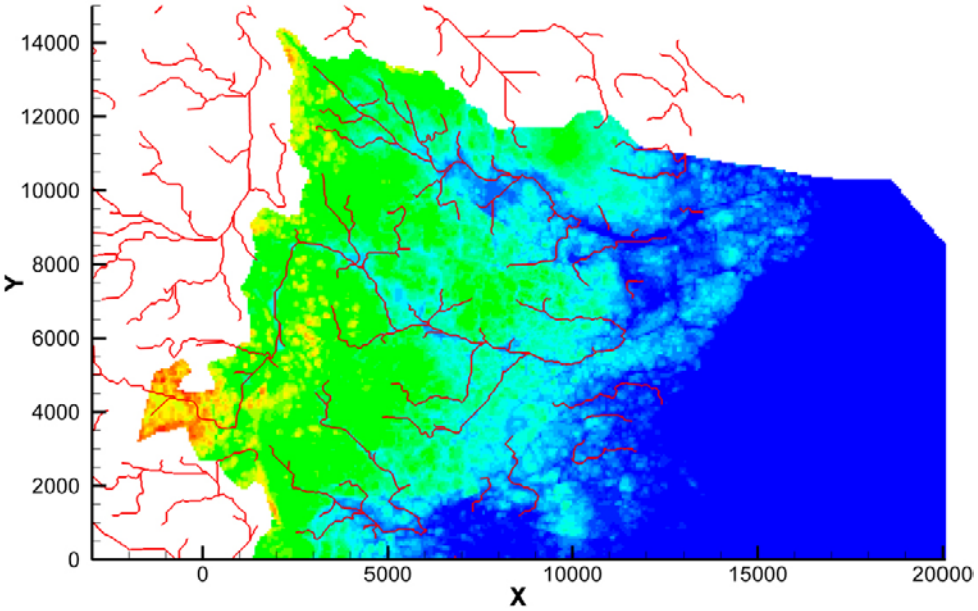

Figure 2-10. *Model domain of the Laxemar DarcyTools model coloured by topography (local model-specific coordinate system in meters). The defined stream network is indicated by red lines.*

2.2.3 Deformation zones

A total of 71 deterministic deformation zones have been modelled in the regional model domain for Laxemar (Figure 2-11). The hydraulic parameterisation of the deformation zones is described in SKB (2009a). The base case model, where the zones were modelled as homogeneous in the lateral direction (but with some local conditioning), was applied in this study. A depth dependency in the hydraulic properties was defined in the vertical direction. The Laxemar hydro-structural conceptual model (SKB 2009a) does not include sheet joints, as modelled in Forsmark, cf. Section 2.1.3.

2.2.4 Hydraulic rock domains

The hydraulic properties of the rock between the deformation zones were in the SDM defined in terms of a stochastic hydrogeological DFN model (SKB 2009a). Based on geologically defined fracture domains (SKB 2009a), the bedrock inside the local model area was divided into a number of hydraulic rock domains (HRD) with different DFN properties, and each hydraulic rock domain was also subdivided into depth intervals. A stochastic DFN was defined in the regional model outside the local hydraulic rock domain as well. One realization of the stochastic DFN for Laxemar, the so-called hydrogeological DFN model base case (SKB 2009a), was imported and applied in this study.

2.2.5 Transport properties

The kinematic porosity of the bedrock was derived from the porosity and geometry of the underlying deformation zone model and the DFN model. The same homogeneous kinematic porosity with a generalised depth trend was used for all deformation zones, and the kinematic porosity of the DFN fractures was derived from the transmissivity through an empirical relationship (SKB 2009a). The resulting porosity field was then the sum of the deterministic porosity field of the deformation zones and the stochastic porosity field of the DFN fractures. A minimum background porosity of $5 \cdot 10^{-5}$ was applied ($1 \cdot 10^{-3}$ in the upper 20 m of the model).

2.2.6 Boreholes

Candidate boreholes

The three core drilled investigation boreholes KLX04, KLX06, and KLX10 in the Laxemar site investigation area (Figure 2-12) were selected as candidate boreholes for the virtual borehole sealing

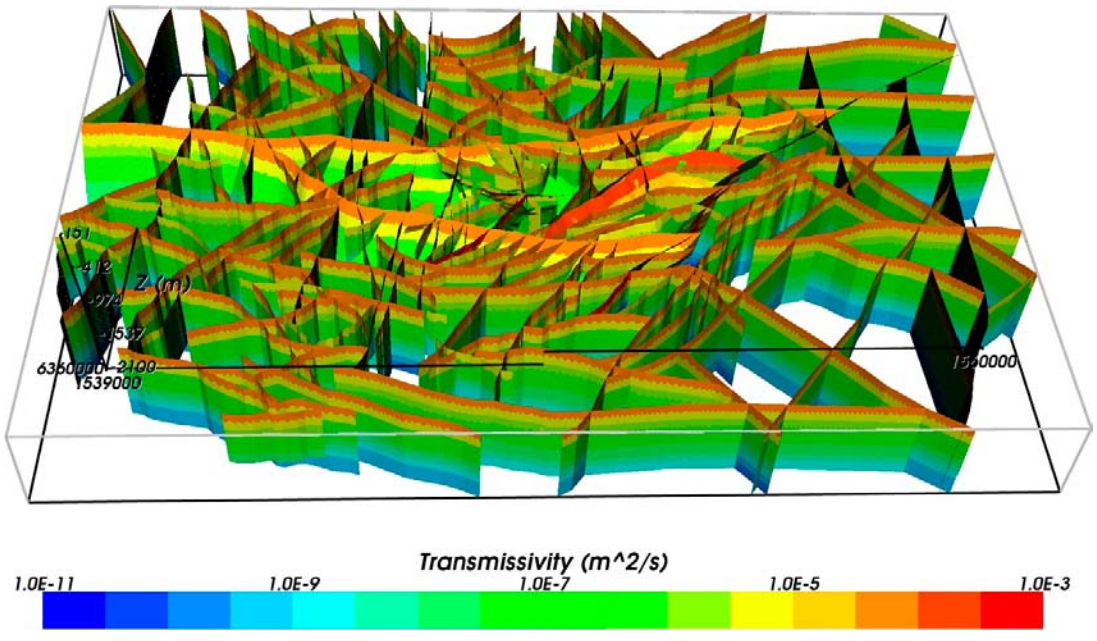

Figure 2-11. *Deformation zone model for Laxemar. The zones are coloured by the transmissivity. (Reproduced from SKB 2009a.)*

study (Pusch et al. 2011). The criteria for the selection of the candidate boreholes were the same as for the Forsmark boreholes, see Section 2.1.6. The borehole KLX06 was selected as a reference borehole for detailed studies and the motivation to include also the other two boreholes was to simulate and investigate the simultaneous effect on the groundwater flow of a number of open boreholes in the area. The locations of the boreholes in relation to the surface traces of the deterministically modelled deformation zones are provided in Figure 2-12, and the intersections of the reference borehole KFR06 and the modelled deformation zones are shown in more detail in Figure 2-13.

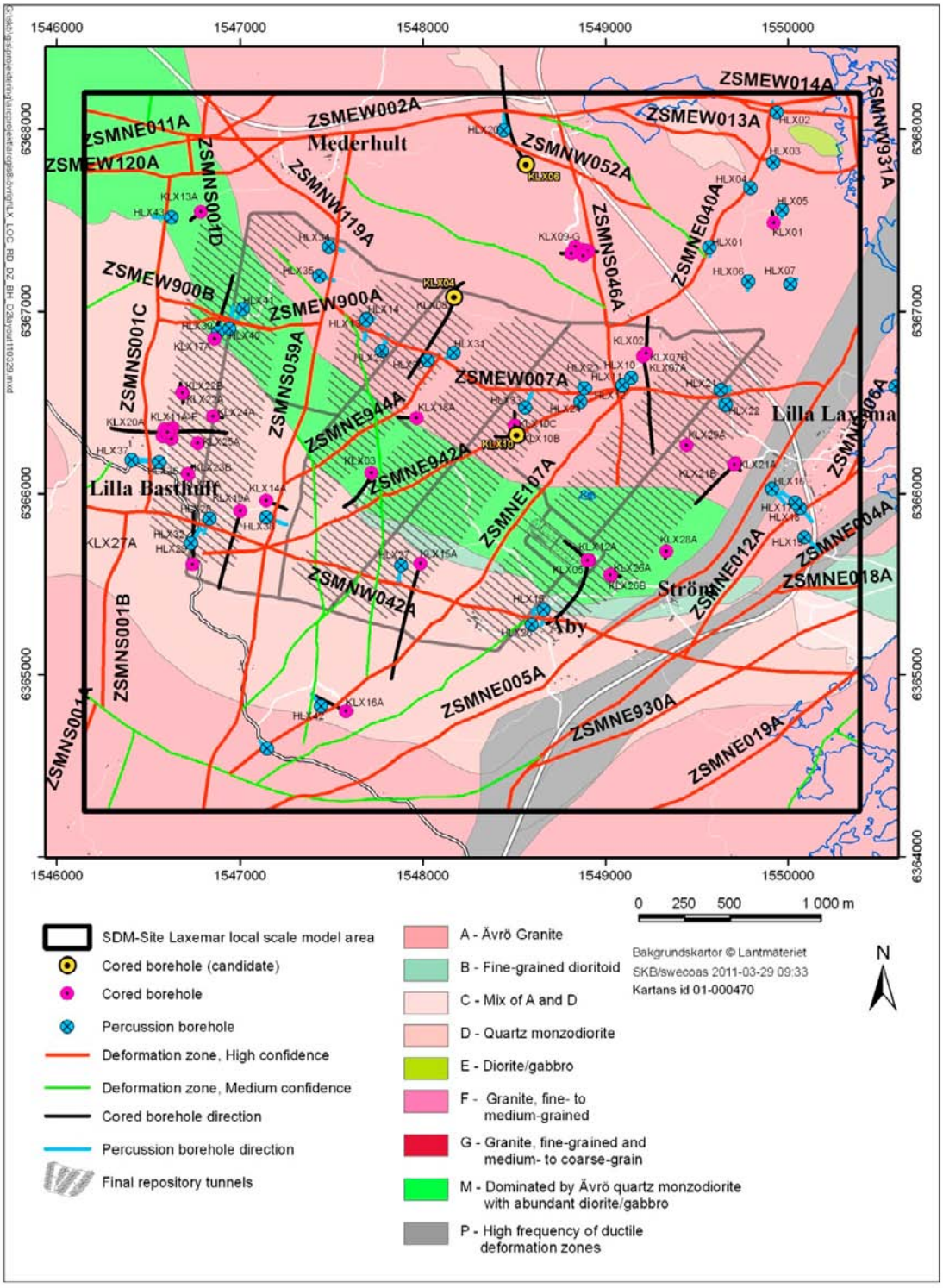

Figure 2-12. *Geology of the Laxemar area and location of the studied (candidate) boreholes in relation to the proposed layout of the final repository (Layout D2).*

Borehole plugs

The borehole sealing concept and the hydraulic properties of the borehole plugs are described above in Section 2.1.6. The developed reference plugging scheme for the borehole KLX06 and a simplified plug version are shown in Figure 2-13.

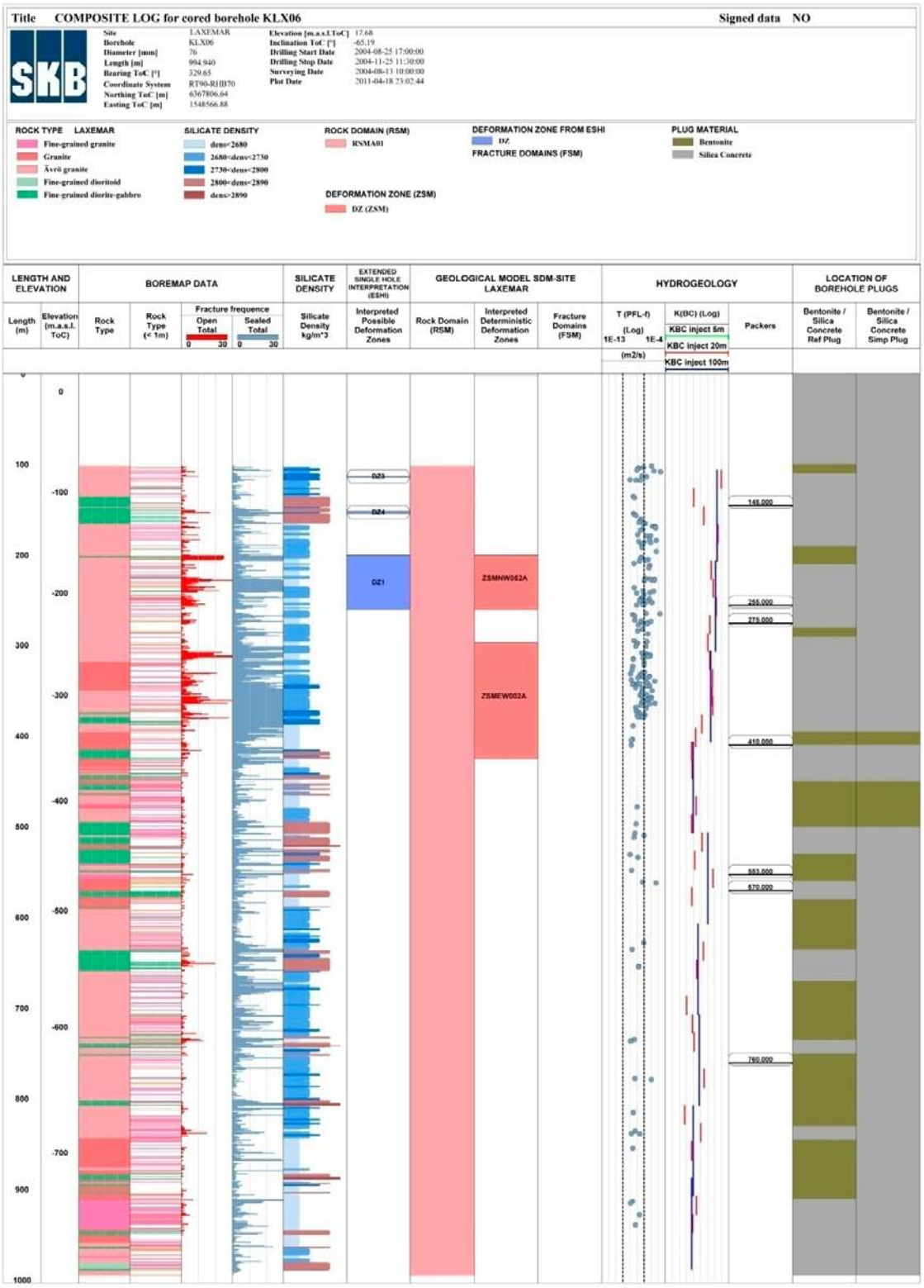

Figure 2-13. *Composite geological and hydrogeological log for borehole KLX06 together with the proposed location (Pusch et al. 2011, Pusch R 2009, personal communication) of borehole plugs. (Ref Plug = reference plug, Simp Plug = simplified plug.)*

2.3 Salinity

The equation for salinity was not solved in this study; hence the salinity, and thus the density, of the groundwater were set as being constant in time. The main reason for this approach was that variable-density flow could not be simulated within the boreholes with the routine for open boreholes available within DarcyTools. However, in the Forsmark model a constant zero salinity was applied for the groundwater above sea level and a salinity of 0.6% was applied below sea level. Therefore there was a difference in density of the groundwater above and below sea level that was constant in time. In the Laxemar model zero salinity and fresh water density was applied in the whole model domain.

3 Computer code

3.1 General description

7The groundwater flow and transport modelling code DarcyTools (Svensson and Ferry 2010) was selected for the simulations in this study. The development of DarcyTools has been commissioned by SKB. The main reasons for the selection of this code were firstly that DarcyTools is one of the codes that have been used in the hydrogeological site modelling for Forsmark and Laxemar. Thus, there were existing model setups for DarcyTools that could be transferred for use in this study (preliminary versions of the models reported in Svensson and Follin (2010) and in Svensson and Rhén (2010), respectively). Secondly, a special routine for simulation of open boreholes in DarcyTools has been developed and tested within the Äspö Task Force for Simulation of Groundwater Flow and Transport (Svensson U 2008, unpublished data).

DarcyTools is a continuum porous-medium type of code. Besides the finite-volume equation solver, the code also contains a number of auxiliary programs, e.g., the programs for the grid generation and the DFN generation (Svensson and Ferry 2010). The properties of discrete features (deterministic deformation zones and stochastic fractures) are represented as continuum grid cell properties in the model. The finite-volume method is used for the solution of the groundwater flow equations.

In the DFN generation process in DarcyTools, the DFN is first generated and all isolated fractures are then removed. A fracture is defined as isolated if is not (i) in contact with the model boundary, (ii) in contact with deterministic structures, or (iii) in contact with other stochastic fractures that are in contact with the former.

3.2 Algorithm for simulation of open boreholes

The method applied for representation of open boreholes in DarcyTools was an implicit representation of the borehole. The hydraulic head in the cells representing the borehole can be set constant along the borehole since the flow resistance in the borehole is negligible. (The equivalent hydraulic conductivity of an open borehole is about 2,000 m/s (Svensson U 2008, unpublished data) which gives a hydraulic gradient of about 10^{-6} for a flow of 1 L/min.) The hydraulic head in the borehole is assigned an arbitrary starting value, and the head is then adjusted until the total inflow to the borehole match the total outflow. The flow along the borehole is thus not calculated explicitly by the numerical model. Instead, the flow along the borehole at a certain borehole length was calculated as the net flow (sum of all in- and outflows) between the borehole cells and the surrounding bedrock cells below that level in the borehole.

An advantage of this method is that it is numerically stable compared to explicit methods where the borehole is represented as a geometric structure with a very high hydraulic conductivity. A disadvantage of the method is connected to particle tracking. As there is no flow along the borehole in the model, a particle that enters a borehole gets stuck there.

4 Groundwater flow model specifications

The DarcyTools models for the Forsmark and Laxemar sites used in this study were transferred from a preliminary version (dated June 2008) of the model reported in Svensson and Follin (2010) and from a preliminary version (dated May 2009) of the model reported in Svensson and Rhén (2010), respectively. The main modifications made were that boreholes were introduced in these setups. Also, since this was a generic study not related to any specific repository layouts, no repository tunnels were included in the models.

4.1 Spatial discretization

4.1.1 Model grid

The model domains described in Sections 2.1.1 and 2.2.1 were discretized by the built-in grid generation program within DarcyTools (Svensson and Ferry 2010). The basic discretization applied was a cell size (side length) of 128 m in both horizontal and vertical direction. The grid was then refined in different parts of the domains according to Table 4-1 (visualized for Forsmark in Figure 4-1). A further refinement was done around the boreholes, see Section 4.1.2. A description of the grid generation process in DarcyTools and the possible setting is found in Svensson and Ferry (2010).

In order to accurately resolve a fracture network on a continuum grid, and to preserve the connectivity properties, at least two criteria must be fulfilled: (I) The grid cell size should be smaller than the spacing of the connected fractures, and (II) the cell size should be smaller than the shortest fractures. These criteria should have been met in the Forsmark model in the model volume outside the fracture domains, where the length of the surface trace of shortest structure was 1,000 m (Section 2.1.4). Inside the fracture domains the cell size of 16 m is comparable to the side length of the smallest fracture of 10 m (Section 2.1.4). The side length of the smallest fracture in the DFN of the Laxemar model was about 18 m. The cell size could also be compared to the frequency of observed flowing features. In Forsmark this frequency is from about 30 features per 100 m in the most intensely fractured rock domain, down to less than one feature per 100 m in the sparsely fractured rock (below 400 m depth) (SKB 2008). In Laxemar there is from 50–60 features per 100 m in the upper 150 m of the bedrock, down to less than one flowing feature per 100 m below –650 m (SKB 2009a).

A more detailed DFN was generated in a zone around the focus boreholes KFM07A and KLX06 (see Sections 4.3.3 and 4.4.3). Within a radius of 20 m from the borehole fracture with side length down to 5 m were generated and within a radius of 10 m fractures with side length to 0.5 m were generated. This could be compared to the size of cells around the boreholes which are successively refined down to 0.0625×0.06250×0.1250 m at the borehole cells itself (Section 4.1.2). The frequency of observed flowing fractures in the fracture domains containing KFM07A is from about one flowing fracture per 3 m in the uppermost part (FFM02) down to less than one flowing fracture per 100 m (FFM01 lower).

Table 4-1. Requirements on the grid resolution.

Grid element	Horizontal resolution (m)	Vertical resolution (m)	Cross 2:1 rule (Y/N)	Long. 2:1 rule (Y/N)
Base	128	128	Y	N
Top surface[1)]	64	2	Y	Y
Vertical boundary	64[2)]	–	Y	N
Rivers	32	2	Y	Y
Borehole site	16	16	Y	Y
Borehole	0.0625	0.125	Y	Y

[1)] The uppermost cell layer.
[2)] The water divide. Refinement applied only for the Forsmark model.

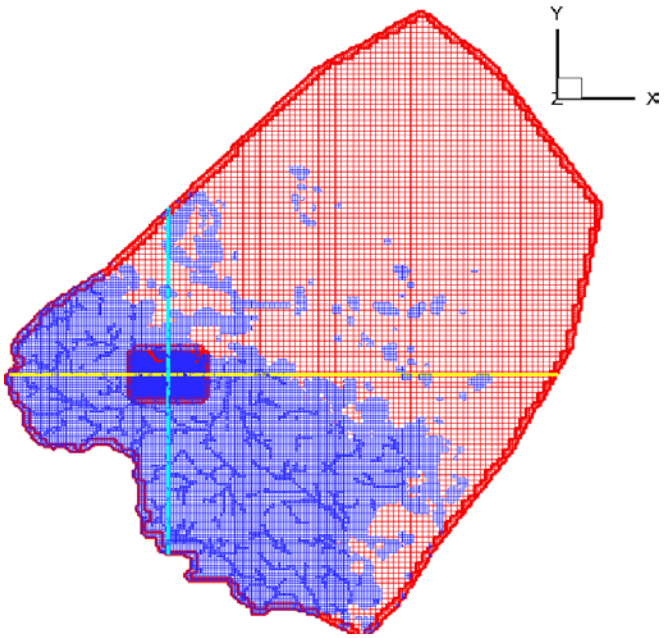

Figure 4-1. *Top view of the Forsmark model grid. The blue-shaded areas are land. The borehole site is the refined area located at the crossing of the yellow and blue profiles.*

The sensitivity of the grid resolution in the Forsmark model setup in DarcyTools on the inflow to an open repository was found to be small in a study by Svensson U (2008, unpublished data). The grid in a box that enclosed the repository was refined from the base cell size 32 m to 8 m. A conclusion that may be drawn from the study by Svensson U (2008, unpublished data) and the discussion about DFN properties above is that the grid resolution in the borehole site volume should be sufficient with respect to upscaling of hydraulic properties from the DFN to the continuum grid.

4.1.2 Borehole discretization

The centre line coordinates with a separation distance of 3 meter along the borehole were obtained from the SKB data base Sicada. The uppermost coordinate that was located in bedrock, according to the borehole information, was used as the start coordinate of the borehole. The part of the borehole located in the soil cover was then left out. The upper part of the boreholes in question is presently cased with a stainless steel casing. However, no casing was considered in this study since the durability of the casing is expected to be relatively short and the casing may even be removed from the borehole in the future. The boreholes were thus modelled as open to the rock over their entire length.

In the grid generation process the grid was successively refined around the boreholes until all cells in contact with the polygon defined by centre lines coordinates had a horizontal side length of 0.0625 m and a vertical side length of 0.1250 m (Figure 4-2, left). These cells were then defined as borehole cells (Figure 4-2, right). The 2:1 size ratio rule (0.125/0.0625) was thus honoured in the refinement process for the borehole cells themselves, but the 2:1 rule was also applied for the cells surrounding the borehole cells. The horizontal side length gives a horizontal area comparable to the cross sectional area of a 0.076 m diameter borehole. The same grid was used for all three simulation cases, i.e., the refinement at the locations of the boreholes was applied also in the case without boreholes.

4.2 Temporal discretization

All simulations were performed as steady-state simulations. The method to reach steady state was successive time-stepping until all simulated control variables appeared to have reached steady-state. The steady-state solution does not depend on the temporal discretization. However, the temporal discretization affects the numerical stability and convergence of the simulations. A basic time step of 1 day was used.

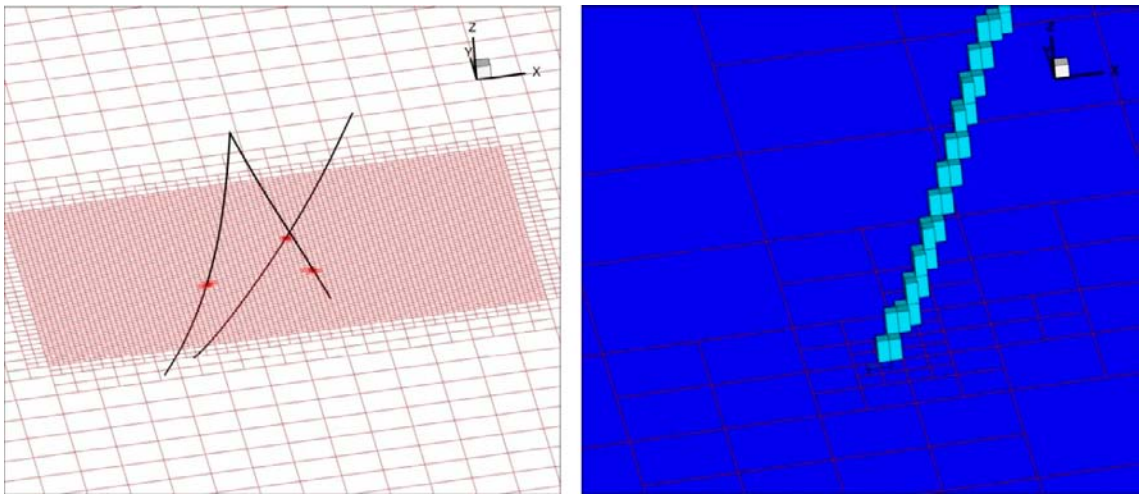

Figure 4-2. *Grid discretization around the studied boreholes in Laxemar (left) and the representation of a borehole as grid cells in 3 dimensions (right).*

4.3 The Forsmark model

4.3.1 Boundary conditions

The original boundary conditions from the imported model setup were used. The vertical boundaries of the model domain consisted of water divides and no-flow boundaries were thus used. A no-flow boundary was also applied at the bottom of the model. For the land-surface cells a specified flux equal to the estimated groundwater recharge (see Section 2.1.2) was used. The position of the free water table is calculated by DarcyTools in an iterative manner (Svensson et al. 2010).

The boundary condition applied in the cells at the sea bottom was a fixed head equivalent to the hydrostatic pressure of sea water with density corresponding to a salinity of 0.6%. The boundary conditions in the open boreholes are described in Section 3.2.

4.3.2 Initial conditions

A steady-state model does not strictly require initial conditions. However, as the method of steady-state simulation in this study was time stepping towards the steady state, initial conditions had to be specified. Also, the initial conditions will affect the numerical stability and convergence properties of the model. The head field for the simulations of natural conditions without boreholes was initialized assuming a vertical hydrostatic equilibrium, and with the water table located 6 m below ground surface (or at sea level as the lowest elevation). The salinity was fixed to zero in all cells above sea level and to 0.6% in all cells below sea level, and the density of the water was set according to the prescribed salinity. The result from the simulation of natural conditions was used as initial condition for the simulations with boreholes.

4.3.3 Hydraulic properties

The deterministic deformation zones and sheet joints described in Section 2.1.3 were employed in the model.

Grid cells that were in contact with the defined stream network (Section 2.1.2) were designated as stream cells. These were given a very high constant horizontal hydraulic conductivity ($K = 1 \cdot 10^{-2}$ m/s). This value was taken from the model setup by Svensson and Follin (2010) and comes from calibrations performed within earlier modelling studies with the DarcyTools model for Forsmark.

Stochastic DFN generation

Fracture domains

A stochastic discrete fracture network was generated inside the fracture domains (Section 2.1.4). The sizes (side lengths) of the generated square-shaped fractures were from 1,000 m down to 10 m. These fractures may represent structures from minor deformation zones down to single fractures. One realization of the stochastic network was applied throughout this study (Figure 4-3).

Detailed DFN around borehole KFM07

A more detailed DFN was generated in a zone around the reference borehole KFM07A. Within a radius of 20 m and 10 m from the borehole, fractures down to a size of 5 m and 0.5 m were generated, respectively. KFM07A penetrates fracture domains FFM02 (top of borehole), FFM01+FFM06, and FFM05 (end of borehole) (Figure 4-4).

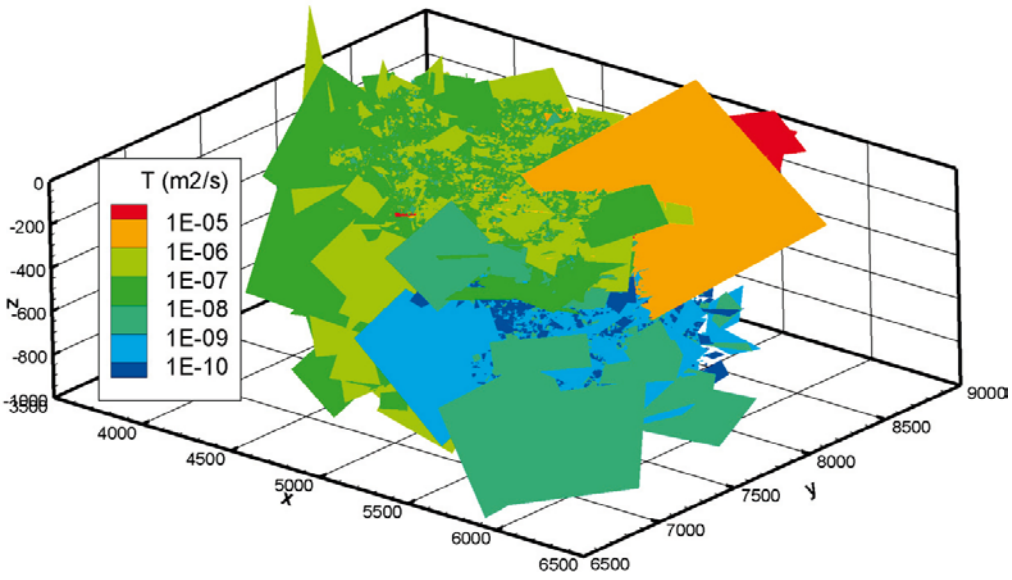

Figure 4-3. *Part of the realization of the stochastic discrete fracture network used in the simulations. Only connected fractures at the borehole site down to z = – 1,000 m (RHB 70) are shown. Fractures in the size interval (side length) 10–1,000 m were generated.*

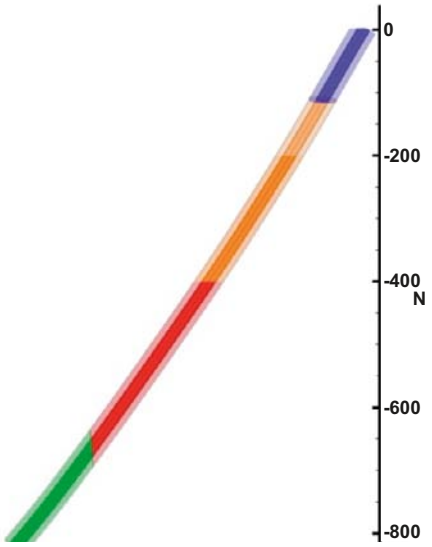

Figure 4-4. *Fracture domains around borehole KFM07A. Blue = FFM02, orange–red = FFM01+FFM06 (upper–middle–lower), green = FFM05.*

The DFN properties of the site resulted in a very sparse connected network around the borehole after removal of isolated fractures (see Section 3.1) in some of the fracture domains. For example, in the lower part of the fracture domain FFM01+FFM06, essentially no connected fractures were left that intercepted the borehole. In contrast, in the surficial fracture domain FFM02 there was a considerably more connected network around the borehole after the removal. However, if the larger (10–1,000 m) fractures were removed, no connected network remained.

Since local isolated fracture clusters that are in contact with a borehole may be of interest as regarding borehole sealing, therefore in this case also all stochastic fractures in contact with the borehole were retained during the fracture sorting process. All stochastic fractures that intersect with the borehole are shown in Figure 4-5. An example of a fracture cluster that connects the level around –200 m in the borehole to a level approximately 50 m lower is shown in Figure 4-6. The stochastic DFN may also be viewed as fracture traces in a plane, an example is shown in Figure 4-7.

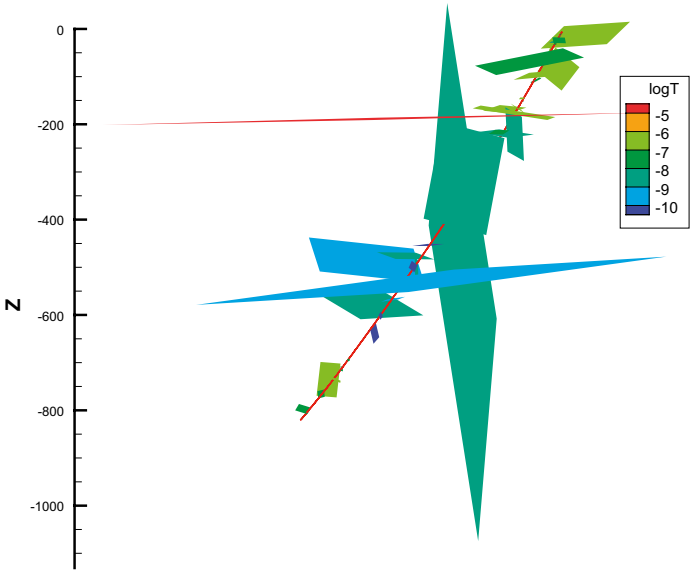

Figure 4-5. *Stochastic fractures intersecting the borehole KFM07A. Coloured by log(T) (m^2/s). Note the extensive high-transmissive stochastic horizontal structure at –200 m. Deterministic sheet joints not shown.*

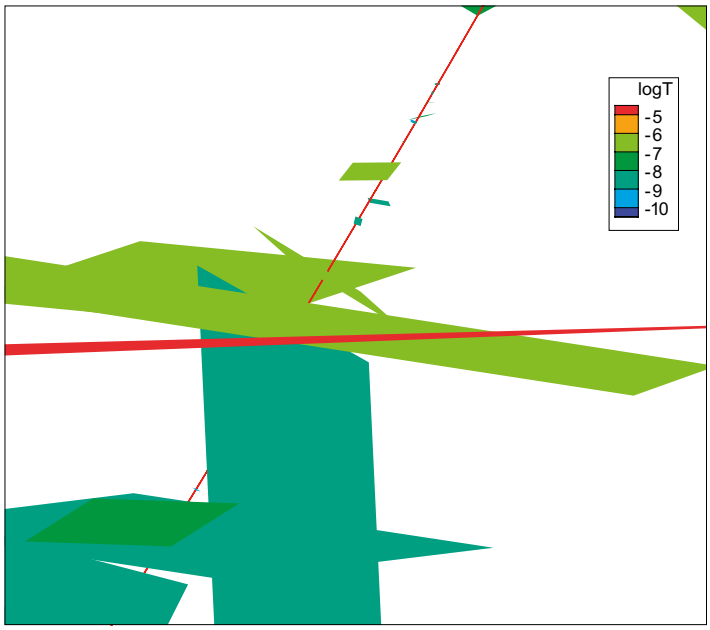

Figure 4-6. *Detail of stochastic fractures crossing the borehole KFM07A at approximately –200 m – –300 m (RHB 70). Coloured by log(T) (m^2/s).*

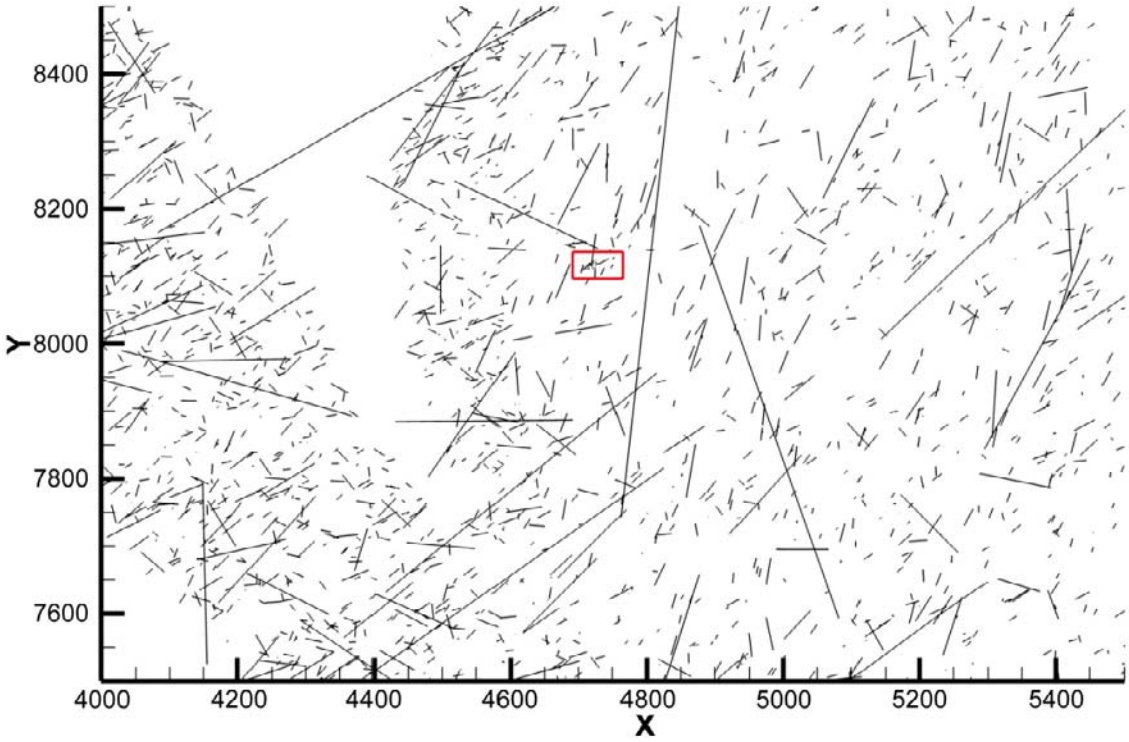

Figure 4-7. *Fracture traces in the plane z = –500 m (RHB 70) at the borehole site (only connected fractures are shown). The empty wedge in the left part of the figure is outside any fracture domain. The red box indicates the detailed DFN generated at the intercept with borehole KFM07A.*

Resulting property fields

First, the deterministic deformation zones and sheet joints and the sorted stochastic fracture network with their individual properties are added to the model, and then the properties of the background rock, i.e., the rock between the fractures and deformation zones, are added. The result is a number of property fields, e.g., hydraulic conductivity (x-, y-, and z-components) and kinematic porosity. An overview of these fields is given in Figure 4-8 and Figure 4-9, respectively. The reason for the large contrast in properties between the cells inside the borehole site volume and the neighbouring cells in the east for the plane at –50 m is that the larger cells outside the borehole site volume cut the sheet joint located at about –70 m, which the smaller cells inside the site volume do not do. The contrast in hydraulic conductivity at depth between the tectonic lens and the surrounding rock is also noticeable (cf. Figure 4-8, lower).

A closer look at the kinematic porosity field in a horizontal plane through the borehole site volume at the level –600 m shows (Figure 4-10) a porosity between 0.001% (the background porosity) and 0.01% (in deterministic deformation zones). The cell size (side length) in the plane (borehole site volume) is about 16 m. Only the deterministic deformation zones are then in practice influencing the porosity, since the connected fracture network is very sparse.

Plugged borehole

The degraded borehole plugs were simulated by the assignment of appropriate hydraulic conductivity values to the grid cells defined as borehole cells. This was done according to the hydraulic conductivity values given in Table 2-2 and the plug locations given in Figure 2-9.

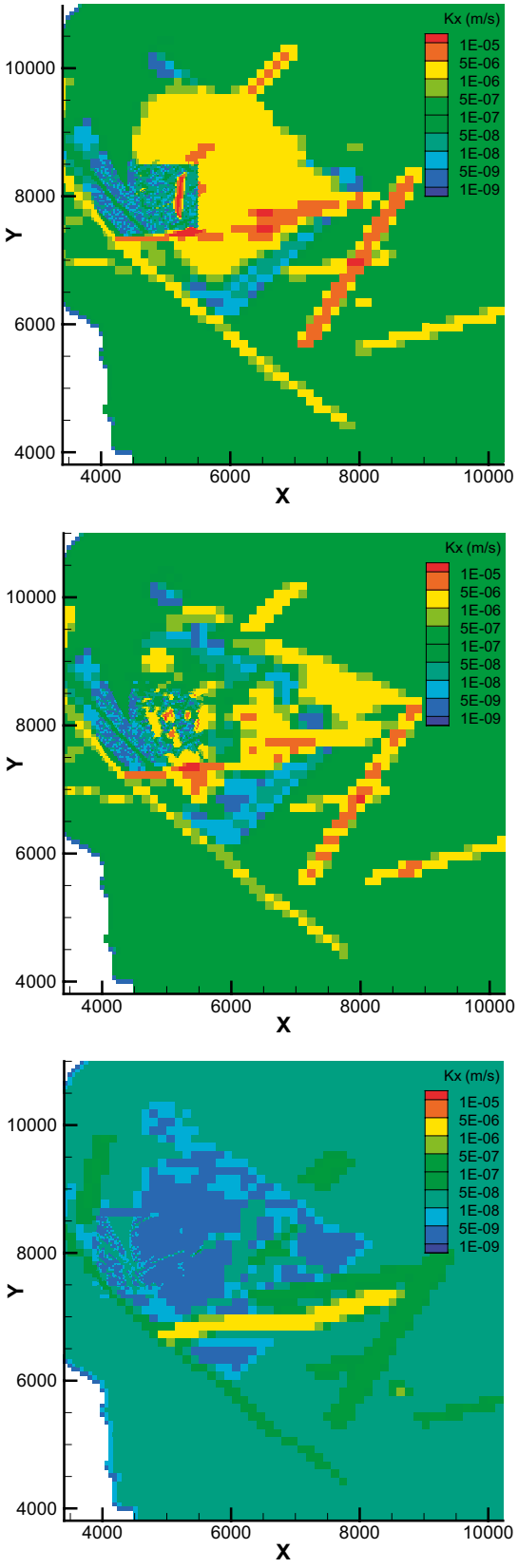

Figure 4-8. *Hydraulic conductivity field (x-component) in the x-y plane at z = –50 m (upper), –100 m (middle), and –400 m (lower). Levels in the RHB 70 system.*

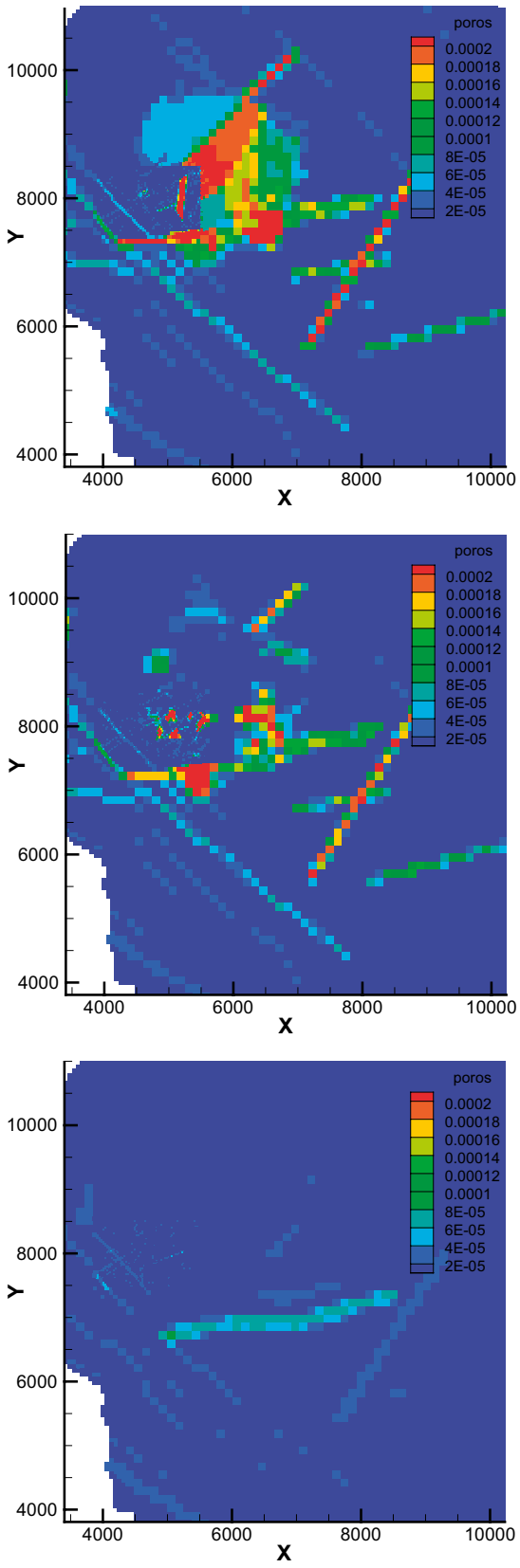

Figure 4-9. *Kinematic porosity in the x-y plane at z = –50 m (upper), –100 m (middle), and –400 m (lower). Levels in the RHB 70 system.*

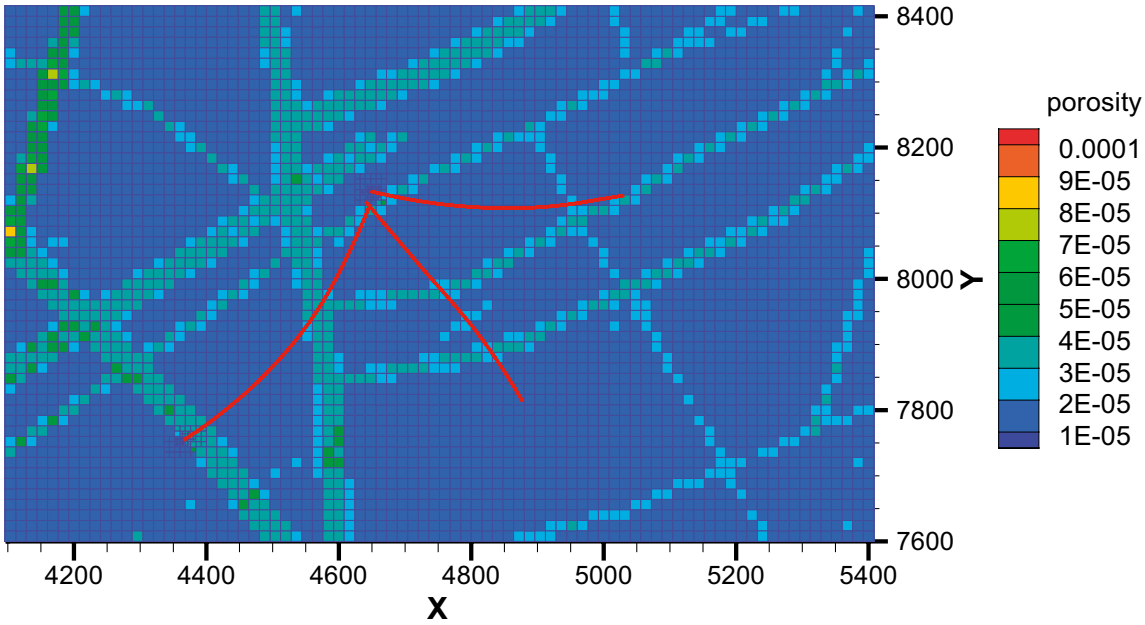

Figure 4-10. *Kinematic porosity in the starting plane for particle tracking at –600 m (RHB 70) in the Forsmark model. The boreholes are projected onto the plane.*

4.4 The Laxemar model

4.4.1 Bondary conditions

The original boundary conditions from the imported model setup were used. Similar to the Forsmark model, a no-flow boundary condition was applied to the vertical and bottom boundaries of the model domain. For the land-surface cells a specified flux equal to the estimated groundwater recharge (see Section 2.2.2) was used, and the position of the free water table was calculated by DarcyTools in an iterative manner. The salinity was fixed to zero in the whole model domain and the boundary condition applied in the cells at the sea bottom was accordingly a fixed head equal to the hydrostatic pressure of sea water with zero salinity. The boundary conditions in the open boreholes are described in Section 3.2.

4.4.2 Initial conditions

The same way as for the simulations of natural conditions without boreholes for Forsmark, the head field was initialized assuming a vertical hydrostatic equilibrium, and with the water table located 6 m below ground surface (or at sea level as the lowest elevation). As mentioned above, the salinity was fixed to zero in the whole model domain. The result from the simulation of natural conditions was used as initial condition for the simulations with boreholes.

4.4.3 Hydraulic properties

The deterministic deformation zones described in Section 2.2.3 (Figure 2-11) were introduced in the model. Grid cells that were in contact with the defined stream network (Section 2.2.2) were designated as stream cells. These were given a very high horizontal hydraulic conductivity that varied linearly with the easting coordinate from about 0.2 m/s in the western part of the domain to about 1.5 m/s in the eastern part. The river conductivity values have been calibrated in earlier studies earlier with the DarcyTools model for Laxemar (Svensson and Rhén 2010).

Stochastic DFN generation

Hydrogeological DFN model base case

The hydrogeological DFN model base case realization (SKB 2009a) covering the whole model domain was imported into DarcyTools (file ls_md2_sets1_64.asc dated 2009-05-05). The sizes (side lengths) of the square-shaped fractures were from 1000 m down to about 18 m. This was a different approach compared to the model setup for Forsmark where one realization of the stochastic DFN was generated within DarcyTools. It should be noted that hence the connectivity to the boreholes was not taken into account when this DFN was generated.

Detailed DFN around borehole KLX06

A more detailed DFN was generated in a zone around the reference borehole KLX06 using the hydrogeological DFN model (SKB 2009a). The applied DFN parameters are given in Appendix 3. Within a radius of 20 m and 10 m from the borehole, fractures down to a size of 5 m and 0.5 m were generated, respectively (Figure 4-11). The DFN generation process is explained in Sections 3.1 and 4.3.3.

Resulting property fields

An overview of the resulting hydraulic conductivity and kinematic porosity fields in the DarcyTools model is given in Figure 4-12 and Figure 4-13, respectively. The hydraulic properties at –50 m and –100 m are similar, but the bedrock at –400 m is less permeable and less porous.

The kinematic porosity at –600 m at the borehole site (Figure 4-14) is between 0.005% (the specified background porosity in the fracture-free bedrock) and about 0.1% (in deterministic deformation zones). A kinematic porosity between the deformation zones above the background value is caused by the stochastic DFN.

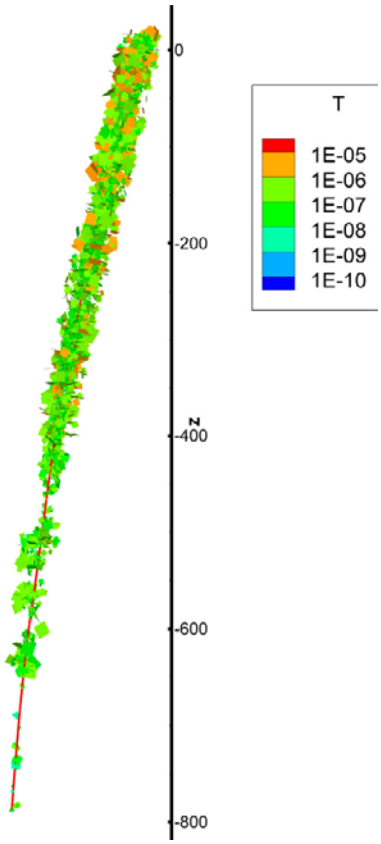

Figure 4-11. *Visualization of the connected fractures of the detailed DFN generated within a radius of 20 m from borehole KLX06.*

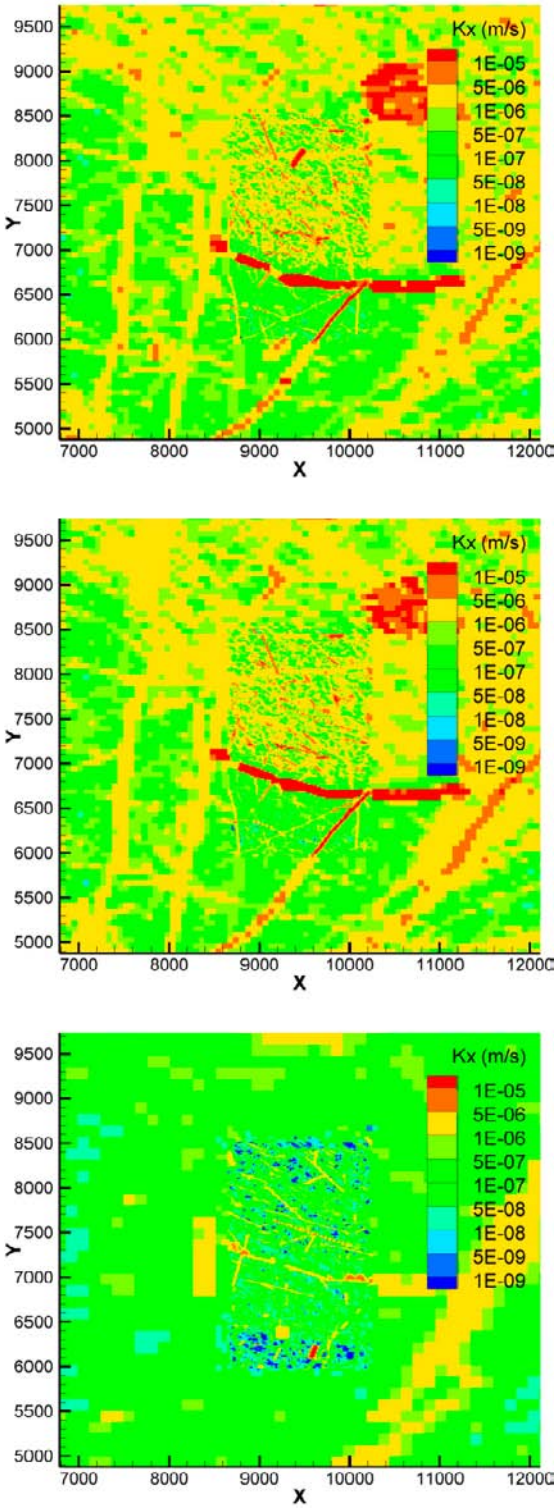

Figure 4-12. *Hydraulic conductivity field (x-component) in the x-y plane at the borehole area in the Laxemar model at z = –50 m (upper), –100 m (middle), and –400 m (lower). Levels in the RHB 70 system.*

Plugged borehole

The degraded borehole plugs were simulated by the assignment of appropriate hydraulic conductivity values to the grid cells defined as borehole cells. This was done according to the hydraulic conductivity values given in Table 2-2 and the plug locations given in Figure 2-13.

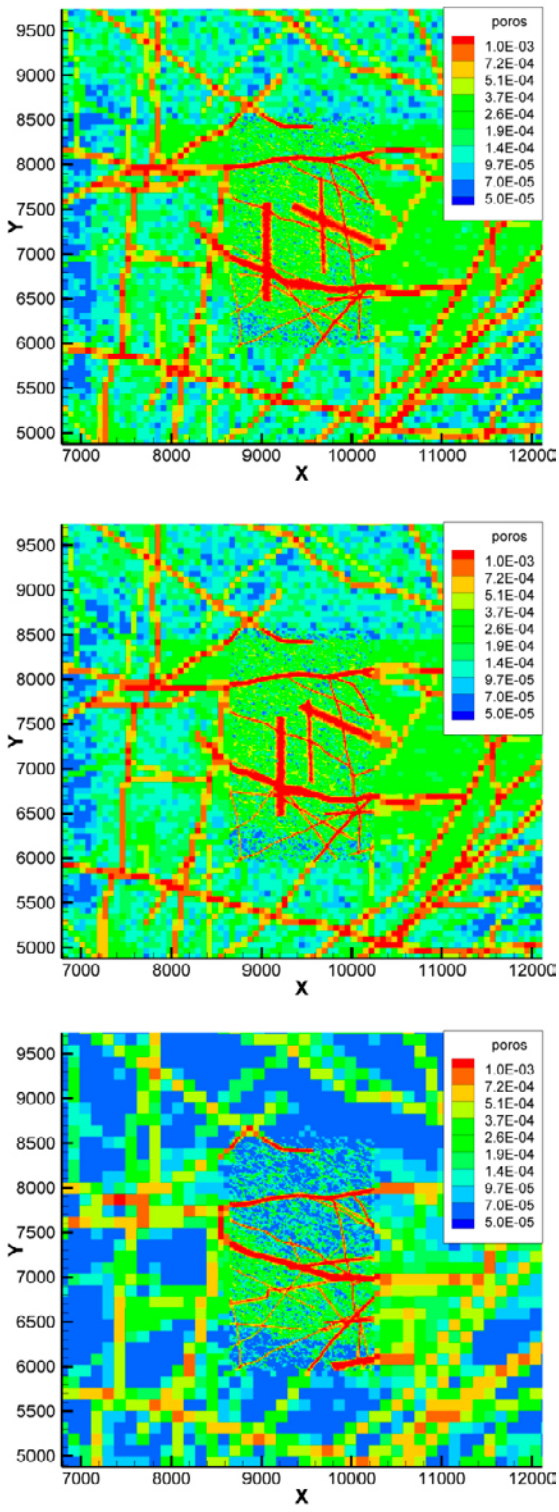

Figure 4-13. *Kinematic porosity in the x-y plane at the borehole area in the Laxemar model atz = –50 m (upper), –100 m (middle), and –400 m (lower). Levels in the RHB 70 system.*

4.5 Partice tracking

In order to study the effect of the boreholes on advective travel time in the bedrock that surrounds the boreholes, particle tracking was performed between a horizontal plane at –600 m (RHB 70) (shown in Figure 4-10 and Figure 4-14) and the –50 m level. The rationale for using these levels was that the particles should be released some distance below the planned repository depth at both sites (–400 to –500 m) and to ensure that the particles were captured below the transmissive surface layer.

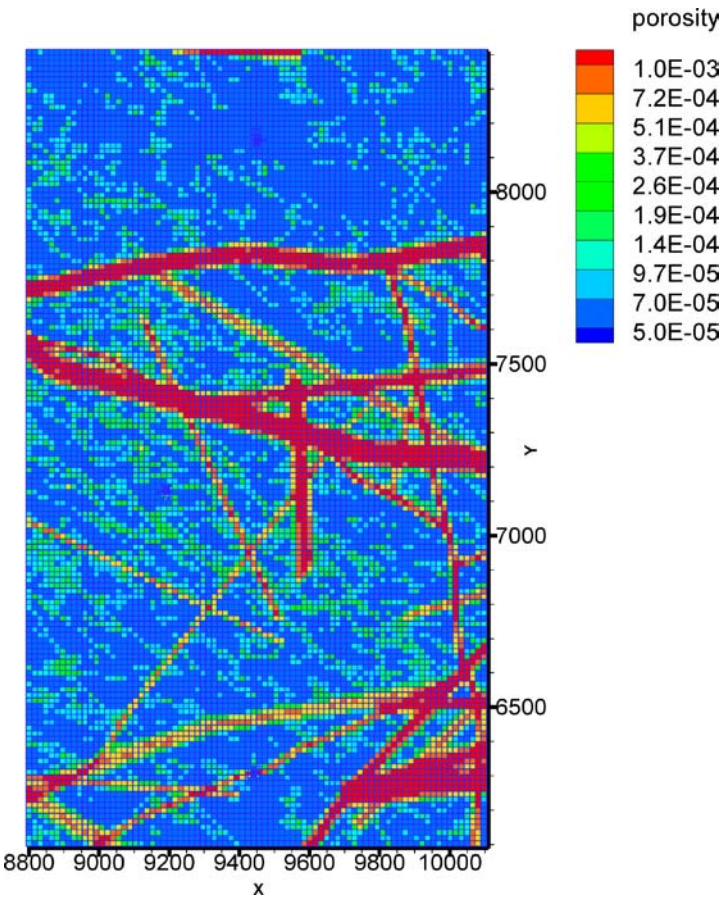

Figure 4-14. *Kinematic porosity in the starting plane for particle tracking at –600 m (RHB 70) in the Laxemar model. The borehole intersections with the plane are marked with circles.*

The starting points for the particles were evenly distributed over the starting plane. A total of 10,000 particles were released which gives a particle density of approximately 1 particle per 100 m^2 across the starting plane. A flow-weighted cell-jump approach was used for the particle tracking (Svensson et al. 2010). Only advective transport was considered.

4.6 Calibration

No calibration of the models was done in the current study since that was outside the scope of the project. However, the near-surface part of the basic model setups has been calibrated to some degree in earlier studies (Svensson and Follin 2010, Svensson and Rhén 2010). They studied the distribution of discharge areas and the discharge from the stream network and found that it was in fair agreement with field observations.

5 Results

The hydraulic impact of the open and poorly sealed boreholes has been studied by predictive forward simulations. The variables that have been investigated are changes in the hydraulic head and flow fields at repository depth, the total flow through a defined rock volume surrounding the boreholes, and the flow along the boreholes. Also the effect on advective transport from repository depth to the surface has been studied.

5.1 Forsmark

5.1.1 Hydraulic head

The natural groundwater flow, excluding borehole effects, at repository depth was from southwest to northeast (Figure 5-1). (Repository depth is shown here as –400 m (RHB 70). It has later been designated as –470 m for Forsmark (SKB 2009b).) The effect of the three open boreholes was clearly visible in the hydraulic head field around the boreholes, especially at depth (Figure 5-2). However, the plugged borehole (reference and simplified plugs) gave no visible effects (not shown).

The radius of influence of the open boreholes (influence defined here as drawdown ≥ 0.1 m) was about 600 m in the horizontal plane at repository depth (Figure 5-3). The drawdown inside the boreholes at this depth was about 2 m. The propagation of the drawdown upwards was reduced by the lowermost of the sheet joint structures. Accordingly, there was an increased head due to the boreholes closer to ground surface (see Section 5.1.3 below). The head increase was 0.1–0.3 m in the boreholes at the –50 m level.

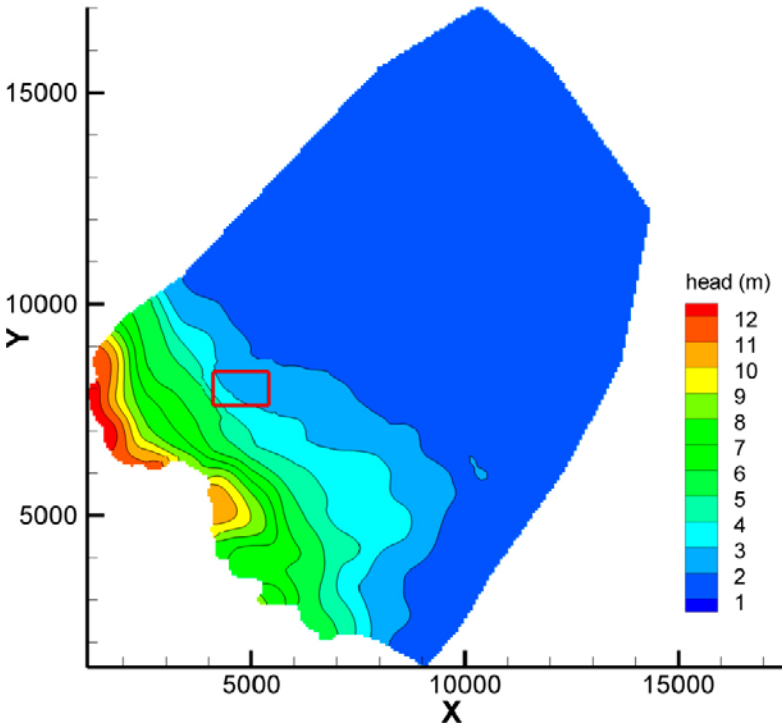

Figure 5-1. *Plan view of the hydraulic head field at –400 m (RHB 70) in the Forsmark model during natural conditions (no boreholes). The borehole site volume is indicated with a red rectangle.*

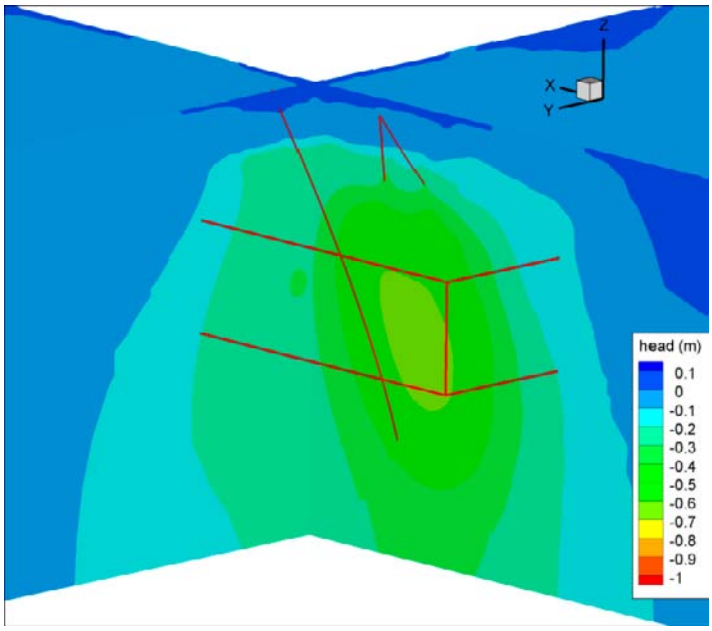

Figure 5-2. *Drawdown caused by open boreholes in the Forsmark model. View from northwest. The borehole site volume is indicated with a red box.*

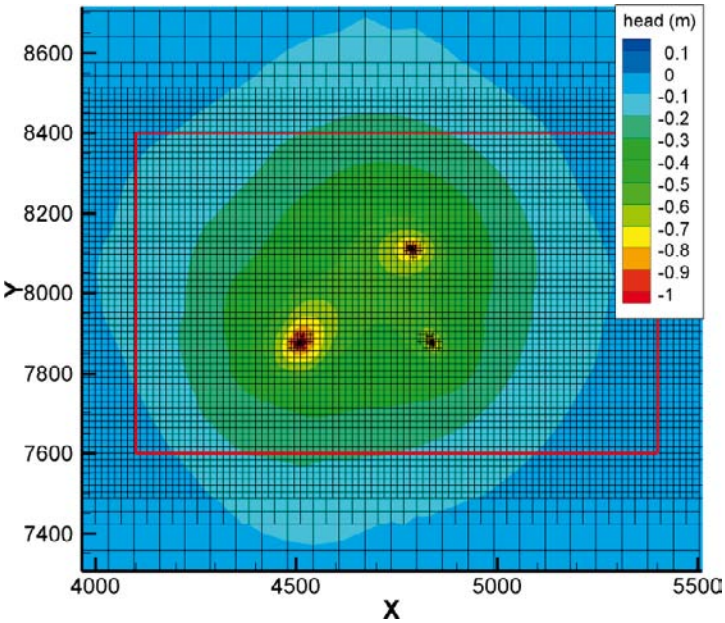

Figure 5-3. *Drawdown caused by open boreholes mapped on the horizontal plane at –400 m (RHB 70) in the Forsmark model. The intersection points of the boreholes are shown as refinements in the grid. The borehole site volume is drawn with a red rectangle.*

5.1.2 Flow field

Specific discharge

The effect on the flow field of the open boreholes was significant (Figure 5-4). The open boreholes increased the connectivity of the fracture system. Many of the high-transmissive fractures would have been less connected without the boreholes. The response was strongly controlled by the high-transmissive structures, especially the sheet joints that intersect the borehole KFM07A.
The change in the specific discharge (Figure 5-4), i.e., the volume of water flowing per unit time through a unit cross sectional area, was some 10% up to some 100% of the natural flow (Figure 5-5)

around the boreholes in the sheet joints and in the transmissive stochastic structure at about –200 m (cf. Figure 4-5). There was an increased flow in some parts of the structures and a decreased flow in other parts. This is due to the fact that it was inflow to the borehole KFM07A from the lowest sheet joint and the structure at –200 m but outflow from the borehole to the two upper sheet joints. There were no visible significant effects on flow field for the plugged borehole (not shown).

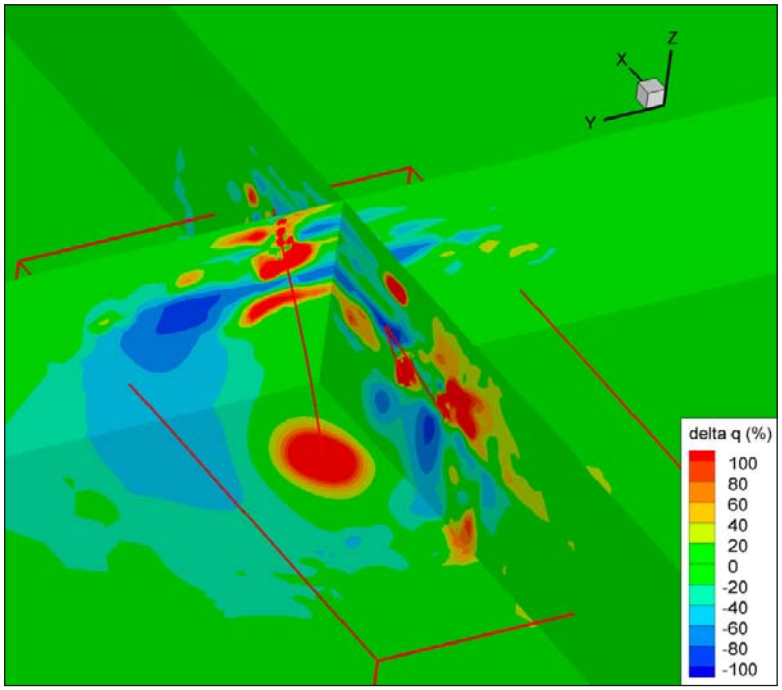

Figure 5-4. *Relative change in specific discharge between the cases no boreholes and open boreholes (positive value indicates increased flow) in the Forsmark model. View from northwest, horizontal plane at the –400 m level (RHB 70).*

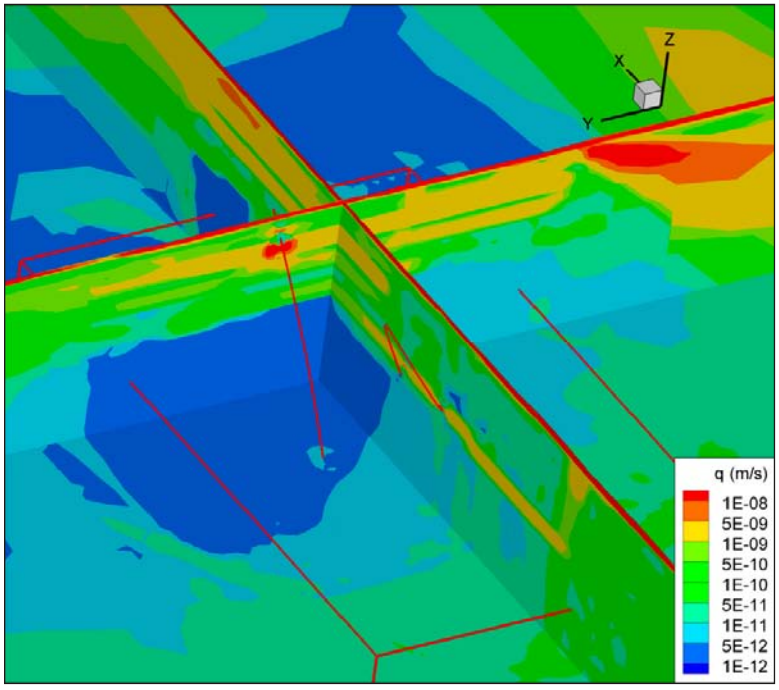

Figure 5-5. *Natural specific discharge (no boreholes) in the Forsmark model. View from northwest, horizontal plane at the –400 m level (RHB 70).*

Flow through borehole site volume

To get a measure of the effect of the boreholes on the total flow through the bedrock at repository depth, the total flow through the borehole site volume (shown in e.g., Figure 5-5) was calculated. The dimension of the volume was 1,300×800 m in the horizontal direction and it extended from –300 m to –600 m in the vertical direction. The computed flows (Table 5-1) are the sums of the in- and outflows over the surfaces of the volume (through the rock itself) and the net flow via the boreholes in to or out from the volume. The open boreholes resulted in an increase of the flow through the rock volume (cross flow through the boreholes not included) with about 17%. The cases with the plugged KFM07A did not differ significantly from the case without boreholes. This is as expected since the conductance of even the degrades silica-concrete sections of the plugged borehole is very small compared to high transmissive fractures.

A large portion of the increased flow comes via the stochastic horizontal structure at –200 m that is connected to the surface via a vertical structure in the western part of the volume (Figure 5-4). Extensive horizontal fractures/sheet joints are expected to occur in the uppermost c. 150 m of the bedrock in the area.

Table 5-1. Flow through borehole site volume in the Forsmark model.

Simulation case	Inflow rock (l/min)	Outflow rock (l/min)	Net outflow through boreholes (l/min)
No boreholes	0.86	0.86	–
Open boreholes	1.01	0.64	0.37
Reference plug KFM07A (degraded)	0.86	0.86	0.00
Simple plug KFM07A (degraded)	0.86	0.86	0.00

5.1.3 Flow along boreholes

Open borehole

The pattern of inflow and outflow along the open boreholes are shown in Figure 5-6 to Figure 5-8. The in- and outflows in all three boreholes were totally dominated by the stochastic horizontal structure at –200 m (see Figure 4-5), and in KFM07A also by the three sheet joints. The open boreholes act as shortcuts between this structure and the conductive shallow bedrock (including the sheet joints).

The maximum flow along the borehole was about four times larger in KFM07A than in KFM09A and KFM09B. This difference is explained by that the sheet joints intersect only KFM07A and not the other two boreholes. It was about the same vertical hydraulic gradient along the boreholes, but the flow along an open borehole is limited not by the flow resistance in the borehole but by the transmissivity of the fractures or deformation zones that it connects.

Plugged borehole

The effect of the plugged borehole KFM07A can be studied by a comparison of the flow between the grid cells defined as borehole cells under natural conditions (no borehole) to the flow when the borehole is plugged (Figure 5-9). The flow shown is the flow across the horizontal faces (z-faces) between two adjacent borehole cells.

There was a more or less continuous flow along the borehole significantly larger than the natural flow only above the –200 m level for both versions of plugs (where there was a silica concrete plug section). This section coincides with the high-flow section in the open borehole (Figure 5-6) where the flow was controlled by a number of high-transmissive structures. The larger flow in the silica concrete sections of the plugged borehole compared to the natural flow is explained by the fact that the hydraulic conductivity of the degraded silica concrete ($1 \cdot 10^{-6}$ m/s) generally is higher than the hydraulic conductivity of the rock (cf. Figure 4-8 and Figure 4-12). However, the flow at the larger fractures and sheet joints in this section was smaller in the plugged borehole than during natural conditions.

The function of the upper bentonite plug immediately below the upper high-flow section in the reference plugging scheme (Section 2.1.6) was important since it isolated it from the flow from below. The simplified plug layout seemed not to be a good solution in this case, since the long silica concrete plug in the section from –178 to –459 m (RHB 70) connected the different fractured sections and provided a long continuous flow path from repository depth and upwards with a flow rate well above the natural. There was a continuous flow upwards also in the more fractured section below about –670 m. However, this section was well isolated from above by the overlying long bentonite plug.

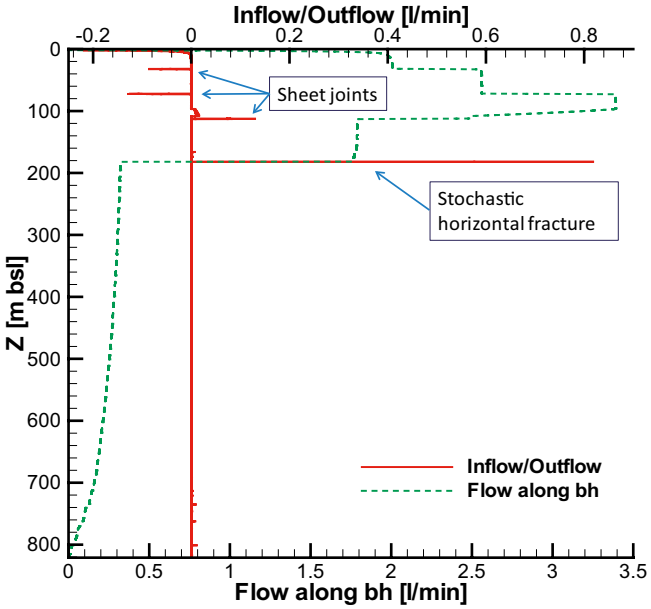

Figure 5-6. *Inflow (+)/outflow (–) and the total flow along the borehole (directed upwards) for the open borehole KFM07A.*

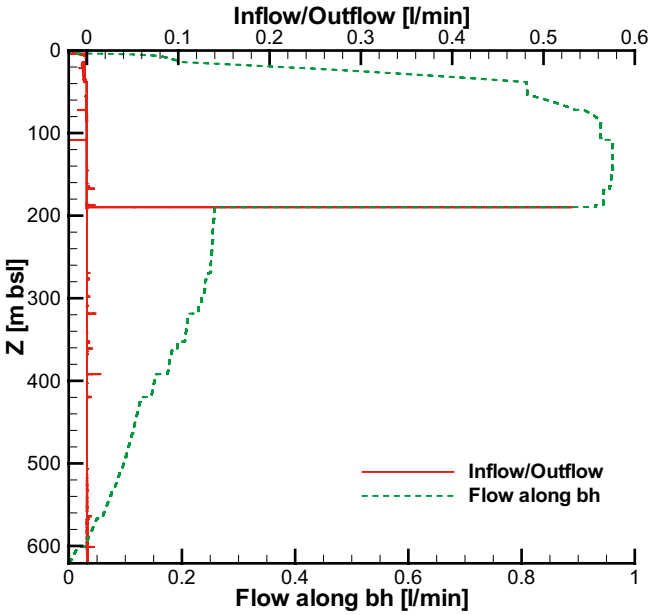

Figure 5-7. *Inflow (+)/outflow (–) and the total flow along the borehole (directed upwards) for the open borehole KFM09A.*

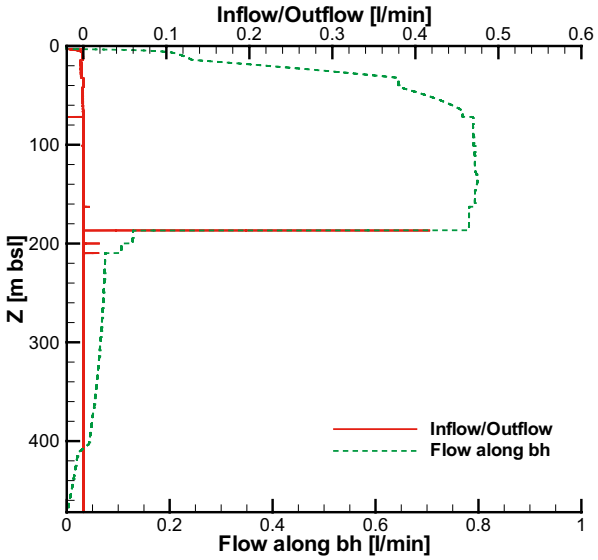

Figure 5-8. *Inflow (+)/outflow (–) and the total flow along the borehole (directed upwards) for the open borehole KFM09B.*

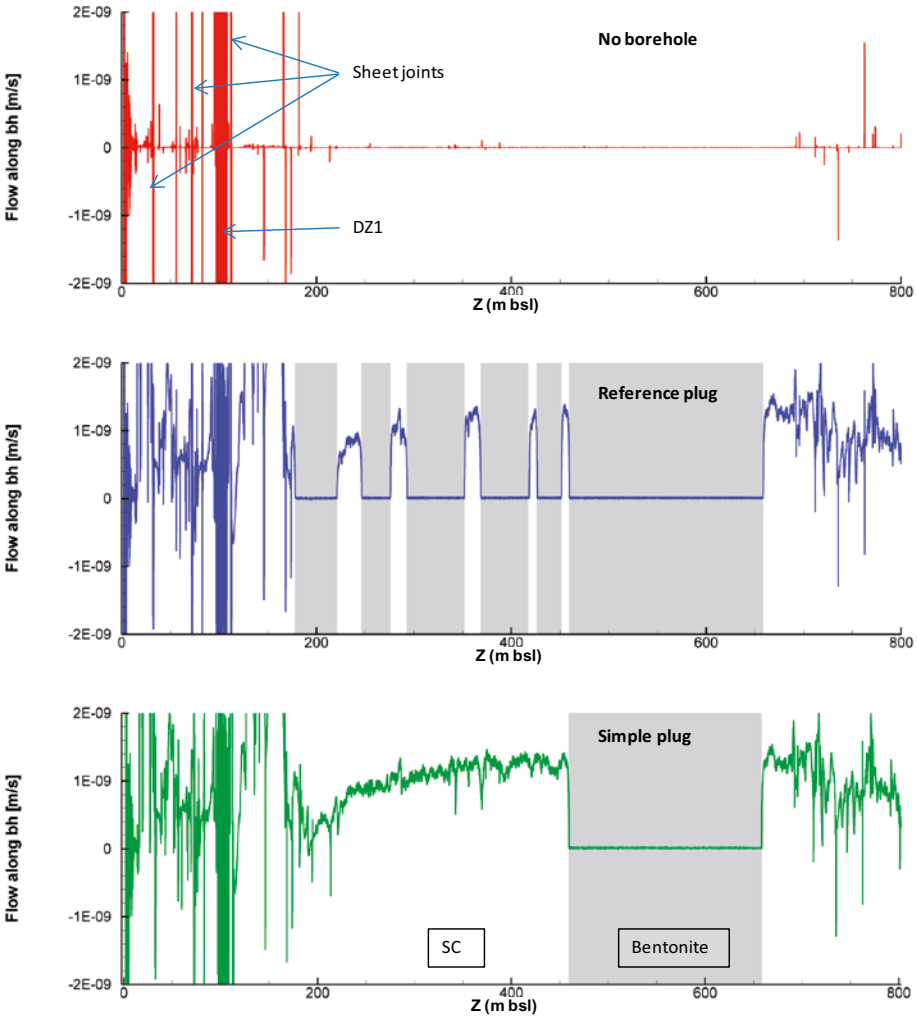

Figure 5-9. *KFM07A. Natural flow (without borehole) in the bedrock along the borehole line (red, upper), along the reference plug (blue, mid), and along the simplified plug (green, lower) (Flow + upwards/– downwards). The bentonite sections of the borehole plugs are shaded gray whereas the rest is silica concrete (SC) sections. DZ1 is the uppermost possible deformation zone interpreted in the single hole interpretation (SHI) of the borehole which is modeled as the deterministic deformation zones ZFM1203 and ZFMNNW0404 in the geological model.*

5.1.4 Particle tracking

Advective travel times between the release area at bottom of the borehole site volume at –600 m (defined in Section 4.5) and the –50 m level was calculated by particle tracking (see Section 4.5) as exemplified in Figure 5-10 and Figure 5-11. In the simulations without boreholes and with a plugged borehole all particles (10,000) reached the –50 m level. The median travel time was about 32 yr, and the travel time of the fastest and slowest particles was about 3 yr and 90 year, respectively (Figure 5-12). The path length varied between about 600 m and 6,000 m, with a median of about 1,500 m (Figure 5-13). Apparently, many of the particles were transported rapidly horizontally in the structure at about –200 m before they reached the surface (Figure 5-10).

There were no significant differences regarding advective transport between the simulations without borehole and with a plugged borehole (Figure 5-12 and Figure 5-13). The flux in the starting plane was in the order of 10^{-12} m/s. Since the kinematic porosity at the –600 m level was about 10^{-5} (Figure 4-10), this resulted in a starting particle velocity of about 10^{-7} m/s or 3 m/yr.

The result of the simulation with open boreholes was quite different. In this case only a fraction, 27%, of the particles reached the –50 m level by way of transport through the bedrock. The rest entered the open boreholes (Figure 5-11). Note that the model could not simulate the transport of the particles within the boreholes after they had entered. However, the flow simulation showed that outflow take place only in the upper c. 50 m of the boreholes (including the two upper sheet joint in KGM07A) (Figure 5-6 to Figure 5-8). Also, a particle that has entered an open borehole (which is open to the surface) is very accessible. Any added travel time and path length for a particle leaving the borehole again for the rock mass at a shallower depth will thus have a lower value from a safety assessment perspective.

Notable is that the travel time of the slowest of the particles (that did not enter the boreholes), and the median travel time, was longer than for the case without boreholes. A hypothesis is that this is an effect of a decreased hydraulic gradient downstream the open boreholes (cf. the area of decreased flow visible in Figure 5-4).

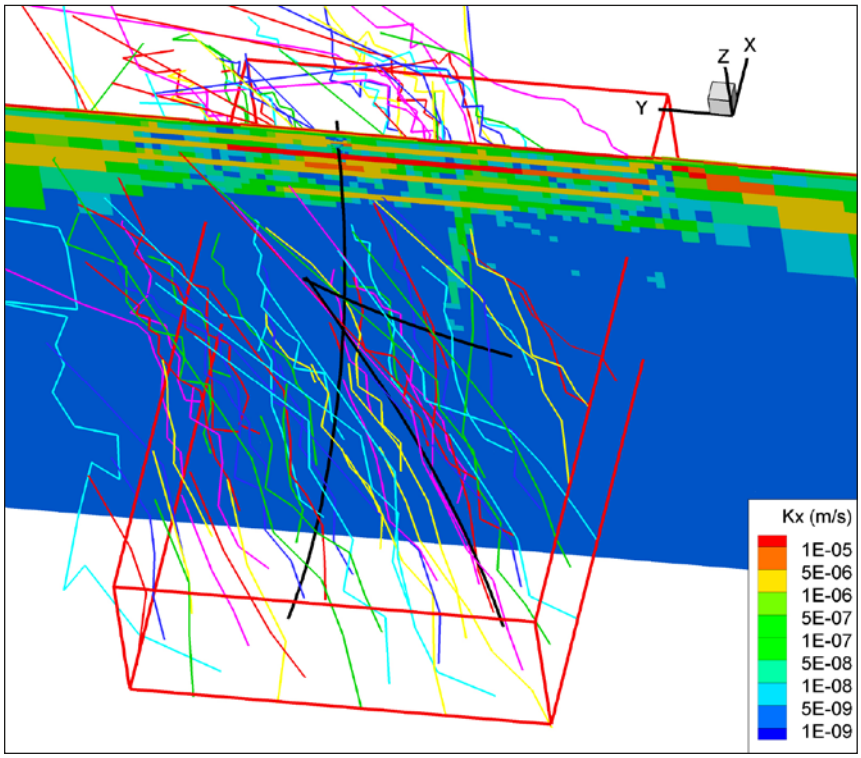

Figure 5-10. *Example of particle trajectories for simulation without boreholes in the Forsmark model at the end of the simulation time at about 100 yr. The vertical plane is colored by hydraulic conductivity. View from west.*

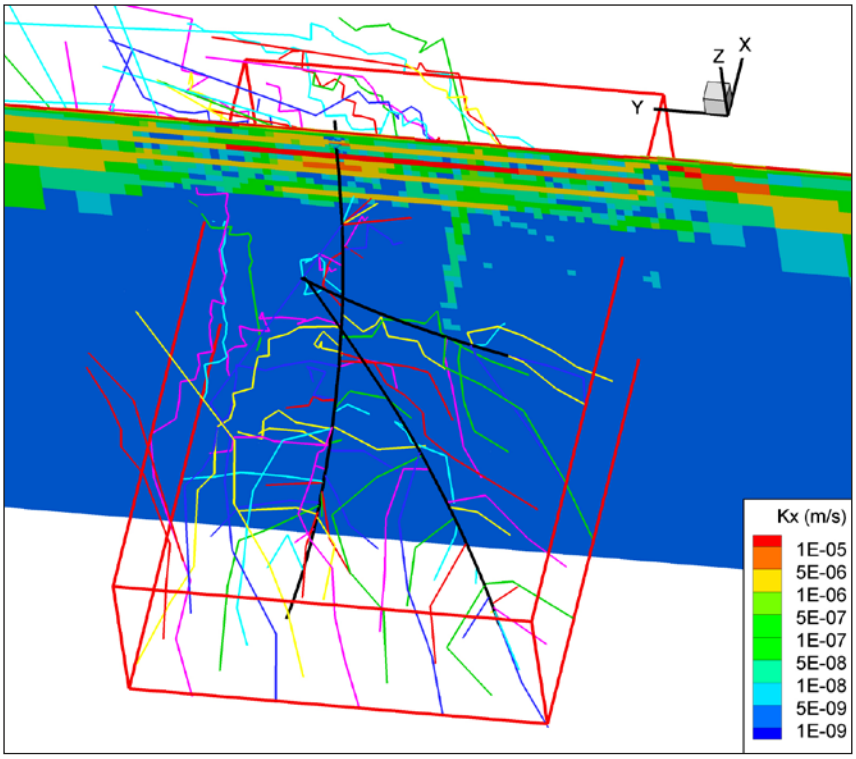

Figure 5-11. *Example of particle trajectories for simulation with open boreholes in the Forsmark model at the end of the simulation time at about 120 yr. The vertical plane is colored by hydraulic conductivity. View from west.*

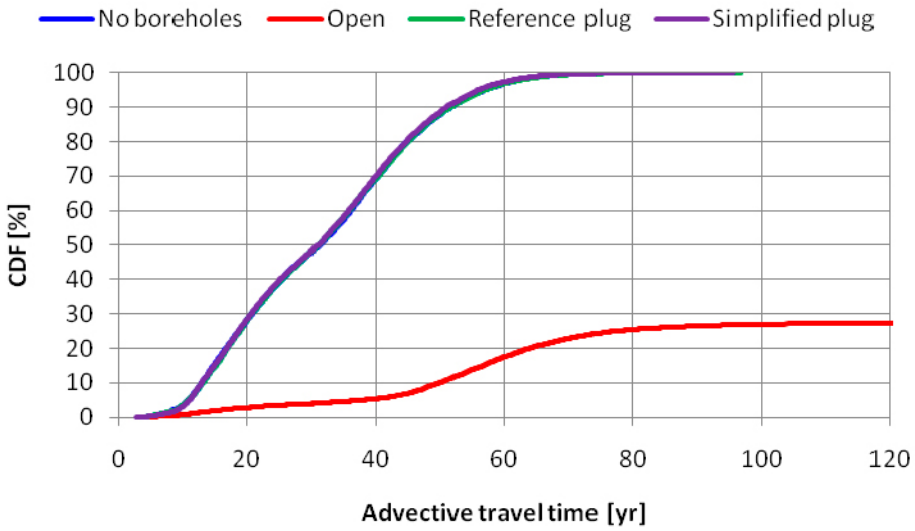

Figure 5-12. *Cumulative density function (CDF) for advective travel times for particles released in the starting plane at –600 m (RHB 70) and captured at the –50 m level in the Forsmark model. The density was calculated as the fraction of the number of released particles. The curves for no boreholes and plugged boreholes are totally overlapping.*

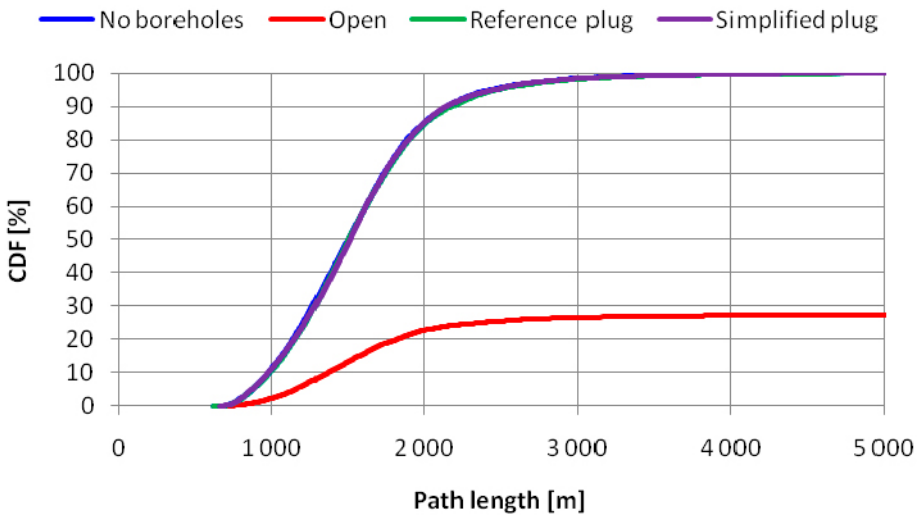

Figure 5-13. *Cumulative density function (CDF) for path length for particles released in the starting plane at –600 m (RHB 70) and captured at the –50 m level in the Forsmark model. The density was calculated as the fraction of the number of released particles. The curves for no boreholes and plugged boreholes are totally overlapping.*

5.2 Laxemar

5.2.1 Hydraulic head

The simulated natural groundwater flow, excluding borehole effects, at repository depth was from west to east (Figure 5-14). (Repository depth is shown here as –400 m (RHB 70). It has later been designated as –500 m for Laxemar (SKB 2009c).) Open boreholes resulted in locally increased head at depth around the three boreholes (Figure 5-15). The maximum radius of influence (influence defined here as drawdown ≥ 0.1 m) was from about 150 m for KLX06 up to about 500 m for KLX10. However, the main influence was seen below repository depth. The only significant influence on head at repository depth was around borehole KLX06 (Figure 5-15, right) where the maximum head increase, inside the borehole, was about 0.9 m. The function of the open boreholes was thus to inject water into the deep bedrock (see also Section 5.2.3 on the flow along the open boreholes). There were no visible effects on head of the plugged boreholes (not shown).

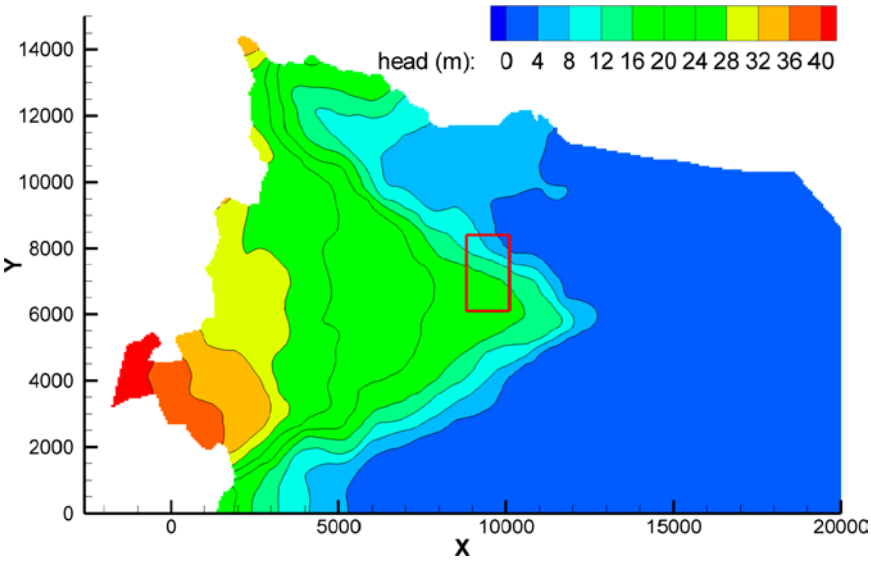

Figure 5-14. *Plan view of the hydraulic head field at –400 m (RHB 70) in the Laxemar model during natural conditions (no boreholes). The borehole site volume is indicated with a red rectangle.*

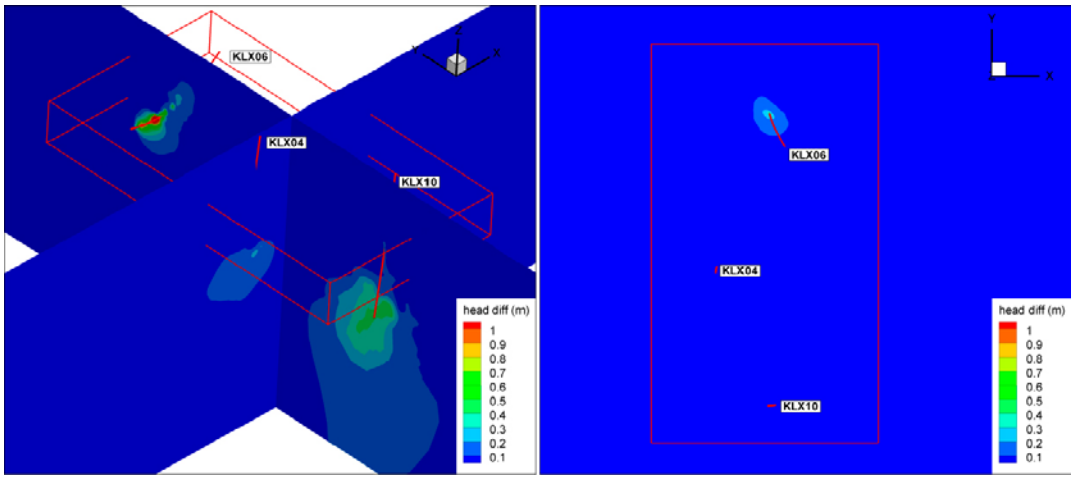

Figure 5-15. *Head change caused by open boreholes in the Laxemar model shown in sections in a perspective view from southwest (left) and in a horizontal plane at –400 m (RHB 70) (right). The borehole site volume is drawn with a red box.*

5.2.2 Flow field

Specific discharge

There was a clearly visible effect on the flow field from the open boreholes (Figure 5-16). The general pattern was an increased flow downstream the boreholes and a decreased flow upstream the boreholes, also at repository depth. This pattern is a consequence of the increased head around the open boreholes. The relative change in specific discharge compared to the situation without the boreholes (Figure 5-17) was typically some 10%, but even up to over 100% in some connected permeable structures close to the boreholes.

Flow through borehole site volume

The defined borehole site volume in the Laxemar model used to study the total turnover of groundwater in the bedrock around the boreholes is shown in Figure 5-16. The dimension of the volume was 2,300×1,300 m in the horizontal direction and it extended from –300 m to –600 m in the vertical direction. The open boreholes resulted in an increase of the total flow through the rock volume (cross flow through the boreholes not included) with about 1% (Table 5-2), where the additional flow was contributed by injection of water from the boreholes. The cases with the plugged KLX06 did not differ significantly from the case without boreholes (Table 5-2).

5.2.3 Flow along boreholes

Open borehole

The pattern of inflows and outflows along the boreholes has been studied for the three boreholes (Figure 5-18–Figure 5-20). The general pattern was inflow into the boreholes from the surrounding rock in the upper c. 100 m and below that outflow from the boreholes to a depth of 300–500 m. The exception is borehole KLX10 where the outflow began directly below surface. Below repository depth the outflow from the boreholes was dominated by flow in a small number of discrete structures. The open boreholes thus act as shortcuts between the uppermost, more permeable part of the bedrock and repository depth.

Table 5-2. Flow through borehole site volume in the Laxemar model.

Simulation case	Inflow rock (l/min)	Outflow rock (l/min)	Net outflow through boreholes (l/min)
No boreholes	98.4	98.4	–
Open boreholes	97.8	99.0	–1.2
Reference plug KLX06 (degraded)	98.4	98.4	0.0
Simple plug KLX06 (degraded)	98.4	98.4	0.0

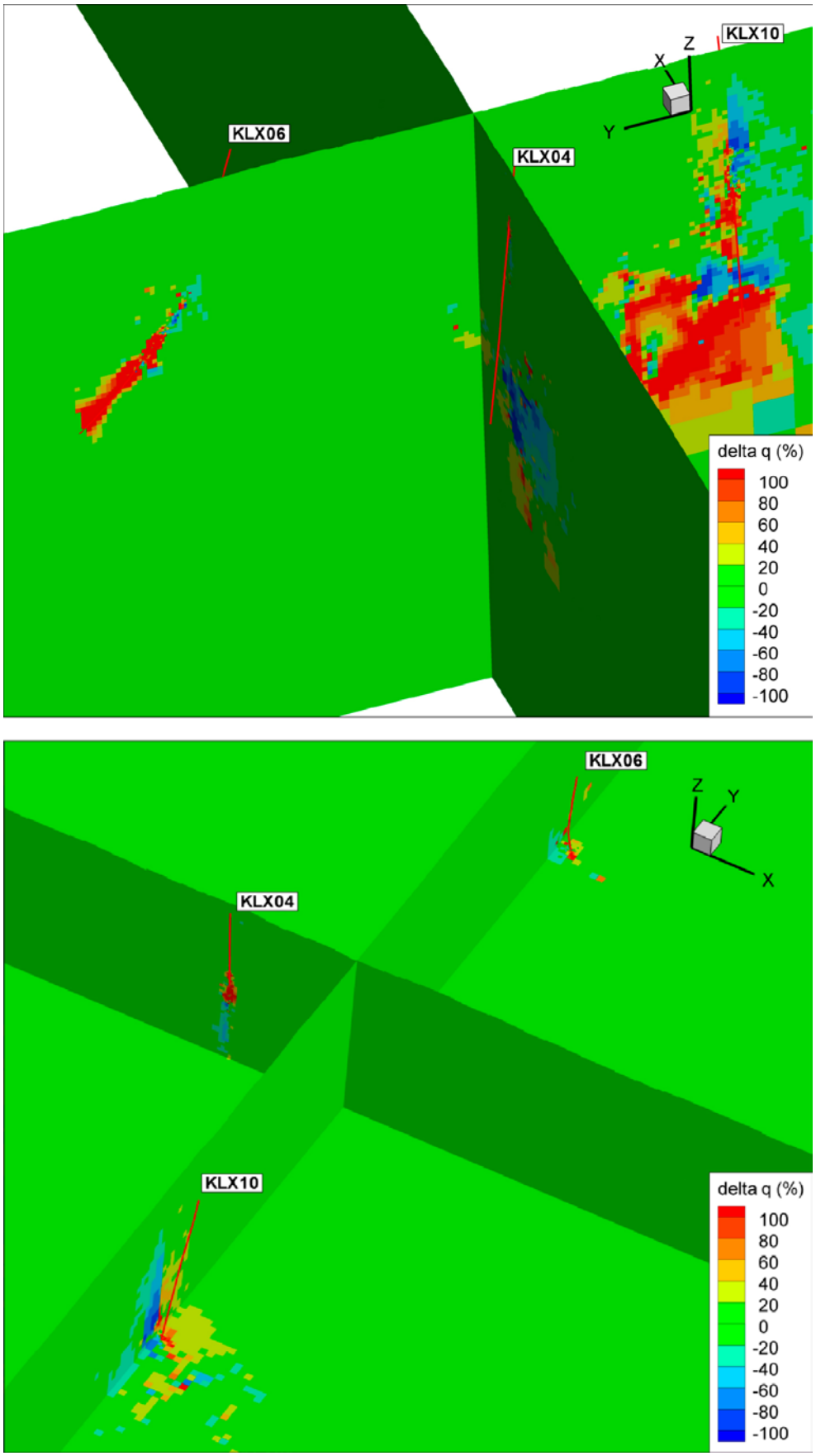

Figure 5-16. *Relative change in specific discharge between the cases no boreholes and open boreholes (positive value indicates increased flow) in the Laxemar model. View from northwest (upper) and from southeast (lower). The horizontal plane in the lower figure is located at –400 m (RHB 70).*

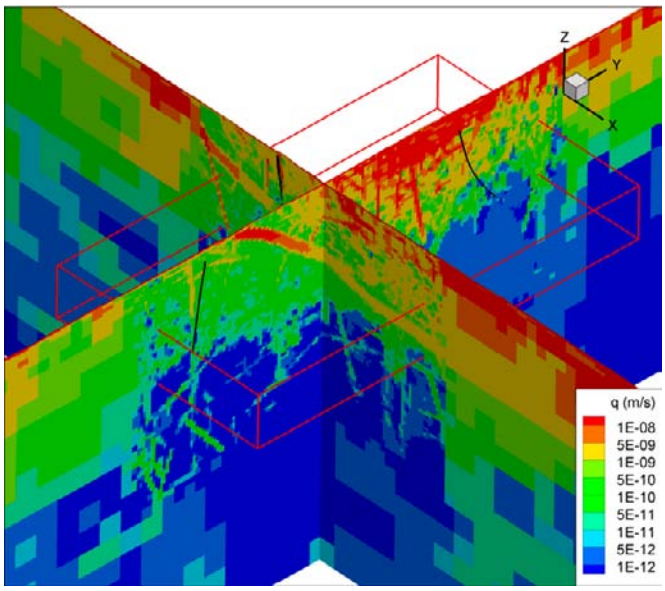

Figure 5-17. *Natural specific discharge (no boreholes) in the Laxemar model. View from southeast. The borehole site volume is drawn with a red box.*

The simulated flow along the boreholes KLX06 and KLX10 was significant. The groundwater flowed from the transmissive surface bedrock into the upper part of the boreholes. The recharge area giving a recharge equivalent to the total flow through these two boreholes was about 3,000 m^2. The inflows and outflows and the maximum flow along the open borehole was about one order of magnitude higher in KLX06 and KLX10 compared to KLX04 (Figure 5-18–Figure 5-20). The reason for this is unclear; the simulated hydraulic gradient over the boreholes is similar, but the difference may be due to stochastic variations in the hydraulic conductivity in the nearfield of the borehole at depth. In reality, the observed total transmissivity of the boreholes is similar for the three boreholes, in the order of 10^{-4} m^2/s (Rouhiainen and Sokolnicki 2005, Sokolnicki and Rouhiainen 2005, Sokolnicki 2007).

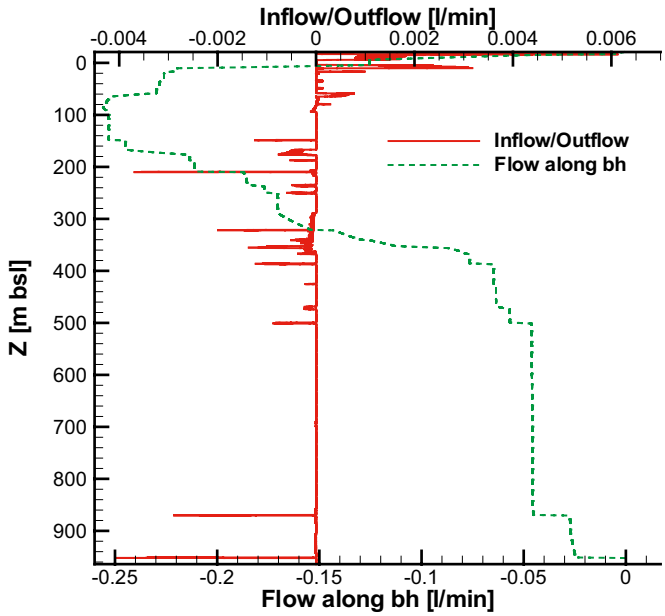

Figure 5-18. *Inflow (+)/outflow (–) and the total flow along the borehole (+ upwards/– downwards) for the open borehole KLX04.*

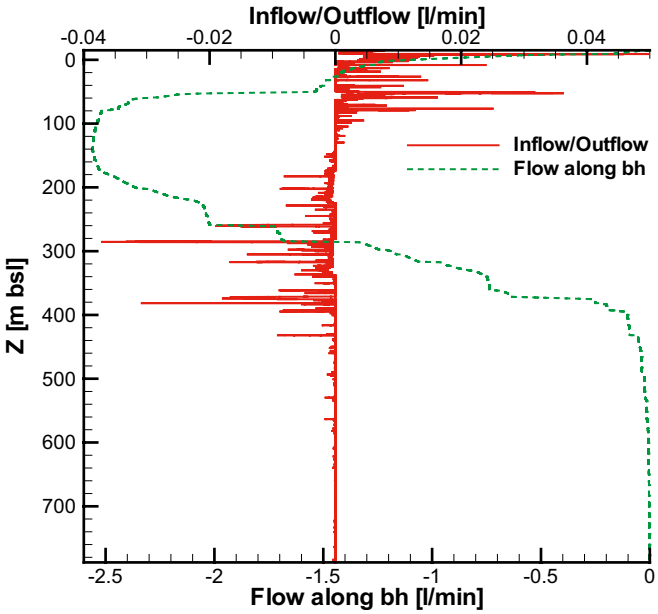

Figure 5-19. *Inflow (+)/outflow (–) and the total flow along the borehole (+ upwards/– downwards) for the open borehole KLX06.*

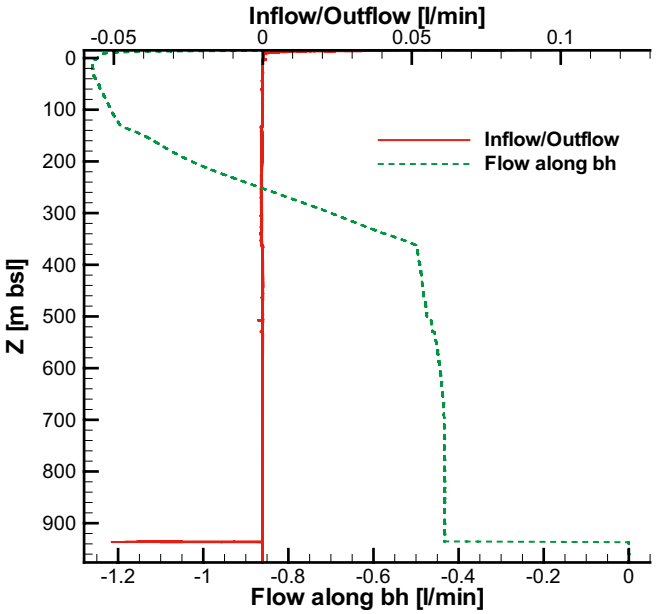

Figure 5-20. *Inflow (+)/outflow (–) and the total flow along the borehole (+ upwards/– downwards) for the open borehole KLX10.*

Plugged borehole

The flow in the uppermost concrete section of the plugged borehole KLX06 (Figure 5-21) was of the same order of magnitude as the natural vertical flow in the bedrock at that depth. In the deeper sections the flow in the concrete sections was significantly higher than the natural flow which decreases with depth from about 10^{-8}–10^{-9} m/s at –150 m to below 10^{-13} m/s at the end of the borehole. In contrast to the situation in the open borehole, there was both upward and downward flow in the plugged borehole. However, no long continuous sections of upward flow were evident.

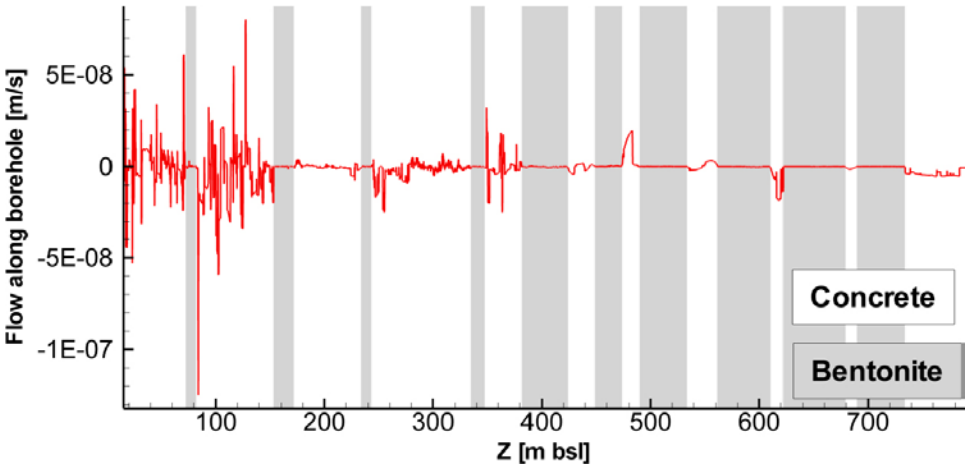

Figure 5-21. *Simulated flow along borehole KLX06 with the reference plug design. The bentonite sections of the borehole plugs are shaded gray.*

5.2.4 Particle tracking

About 95 % of the particles that were released at the bottom of the borehole site volume at –600 m had reached the –50 m level at the stop of the simulation at a time of about 2,000 yr for all simulation cases (exemplified in Figure 5-22 and Figure 5-23)). No particles entered the open boreholes. There were no significant differences in the statistics of advective travel time or path length between natural conditions (without boreholes) and the simulations with plugged borehole (Figure 5-24 and Figure 5-25). The median travel time was about 50 yr for all cases, and the 10%- and 90%-percentile was about 6 yr and 1,000 yr, respectively. There was a difference in travel time between the open borehole case and natural conditions for particles with travel time above about 100 yr, where the travel times of the slowest particles were about 20% shorter in the open borehole case compared to that of natural conditions. The median path length was about 2,600 m, and the 10%- and 90%-percentiles was about 1,400 m and 6,000–7,000 m, respectively (Figure 5-25).

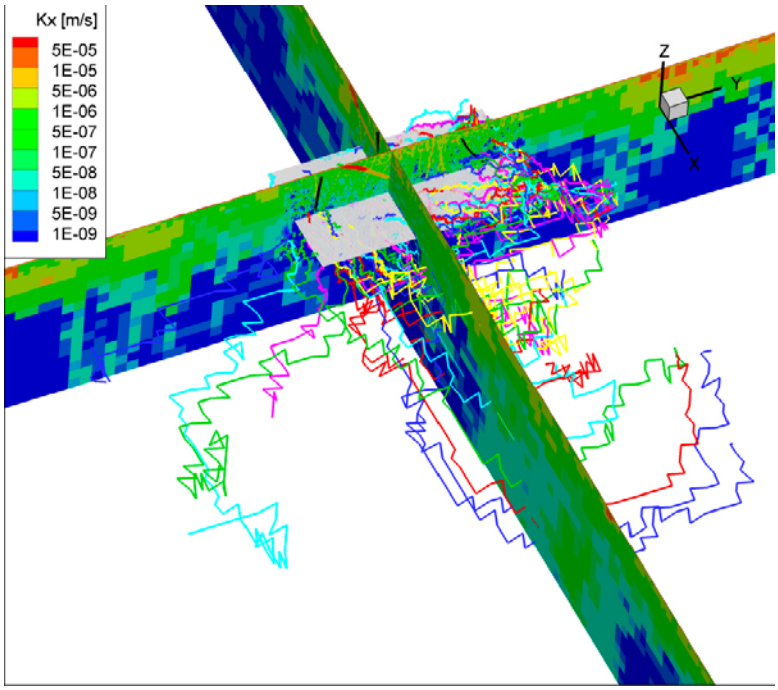

Figure 5-22. *Example of particle trajectories for simulation without boreholes in the Laxemar model at the end of the simulation time at about 2,000 yr. The angular appearance of the trajectories is a result of the cell-jump particle tracking method. The vertical planes are colored by hydraulic conductivity. View from southeast.*

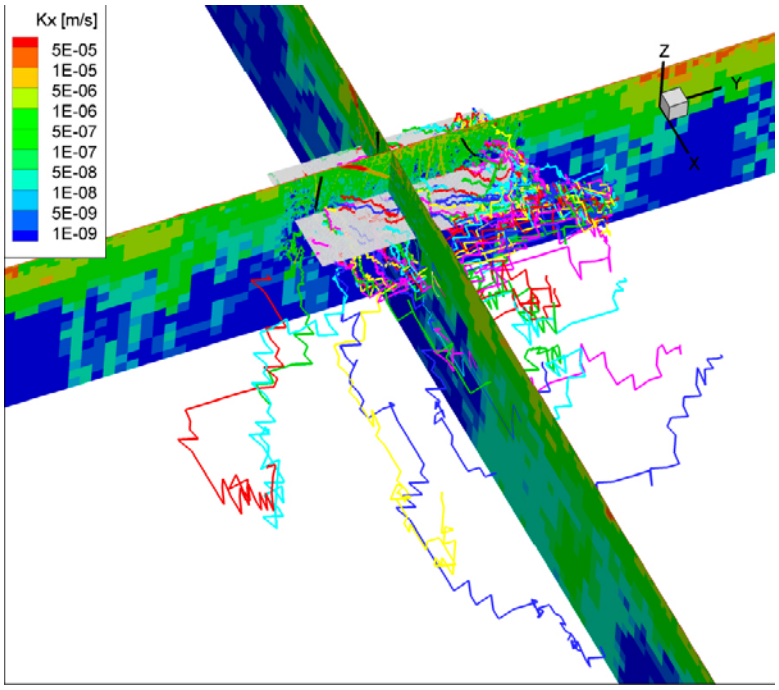

Figure 5-23. *Example of particle trajectories for simulation with open boreholes in the Laxemar model at the end of the simulation time at about 2,000 yr. The vertical planes are colored by hydraulic conductivity. View from southeast.*

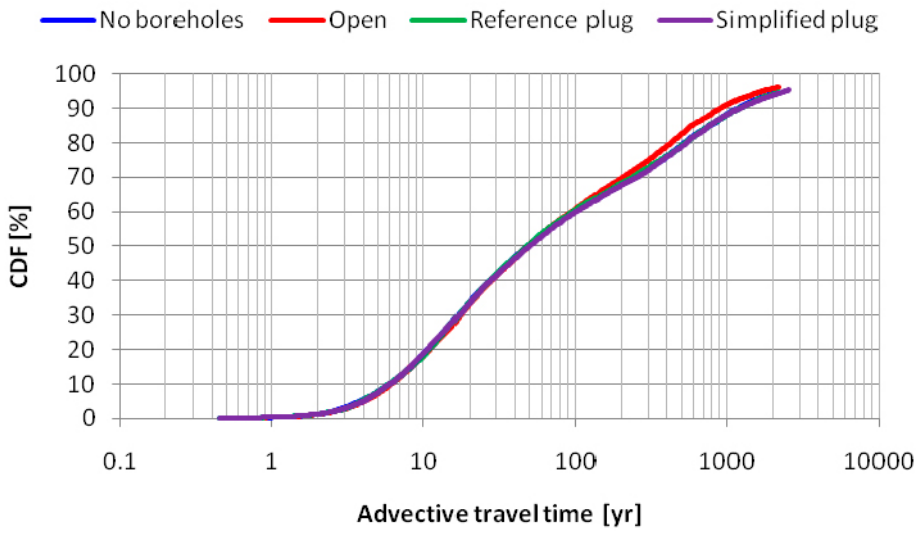

Figure 5-24. *Cumulative density function (CDF) for advective travel times for particles released in the starting plane at –600 m (RHB 70) and captured at the –50 m level in the Laxemar model. The density was calculated as the fraction of the number of released particles. The curves for no boreholes and plugged boreholes are totally overlapping.*

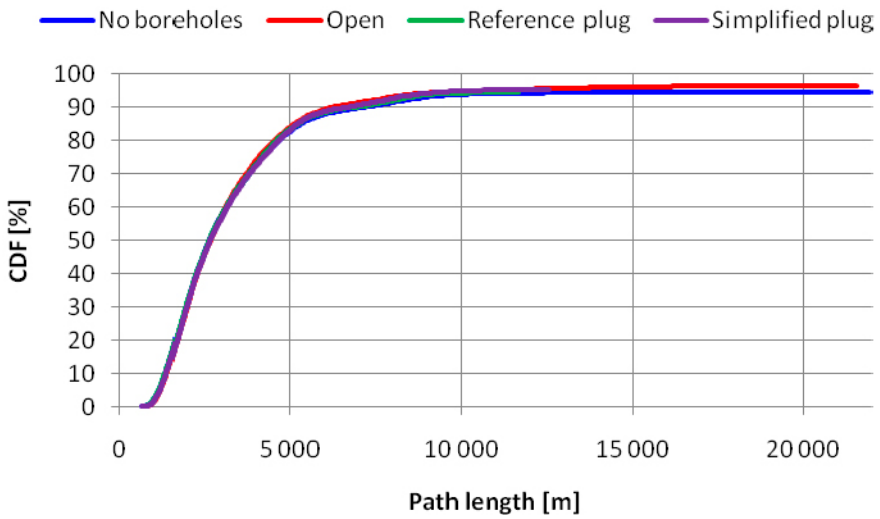

Figure 5-25. *Cumulative density function (CDF) for path length for particles released in the starting plane at –600 m (RHB 70) and captured at the –50 m level in the Laxemar model. The density was calculated as the fraction of the number of released particles.*

6 Discussion

6.1 Hydraulic performace of unsealed boreholes at the two sites

It should be noted that no absolute quantitative evaluations of the performances of the two sites, or strict quantitative comparisons between the two, should be made based on the presented results. It is the results of open and sealed boreholes respectively that should be compared to the results from the situation without boreholes for each site. The quantitative results are completely dependent on the applied hydrogeological conceptual models, and for example the transport properties were not elaborated in this study. However, the qualitative differences between the two sites are regarded as important results that illustrate the possible hydraulic function of open boreholes. The effect on performance measures of the presence of open boreholes close to the intended final repository in Forsmark is quantified by Joyce et al. (2010) as a basis for the assessment of the long-term radiological safety of the repository.

The results show that there is a difference in the hydraulic function of open investigation boreholes when comparing the Forsmark and Laxemar sites for the present-day hydraulic boundary conditions. In Forsmark, as a discharge area for deeper groundwater, open boreholes may acts as easy path ways for groundwater from repository depth to surface. In Laxemar, on the other hand, being in part a recharge area for deeper groundwater, open boreholes may act as paths from surface to depth. The magnitude of the simulated vertical hydraulic gradient is also lager in Forsmark compared to Laxemar. Another difference between the two sites is that the much lower permeability at repository depth in Forsmark compared to Laxemar (cf. Figure 4-8 and Figure 4-12) makes the effect of the open boreholes more apparent in Forsmark. The increased flow through the borehole site volume due to open boreholes is about 17% in Forsmark compared to only about 1% in Laxemar. The sizes of the studied control volumes are of the same order, about $3 \cdot 10^8$ m^3 and $9 \cdot 10^8$ m^3 in the Forsmark and Laxemar cases, respectively, which means that the observed difference in response on total flow is not explained by difference in size between the two studied volumes. However, in absolute numbers is the flow increase in Laxemar larger, since the simulated specific flow through the borehole site volume is only $5 \cdot 10^{-14}$ m^3/(m^{3}s) in Forsmark compared to $2 \cdot 10^{-12}$ m^3/(m^{3}s) in Laxemar.

The difference in the hydraulic function of the open boreholes between the sites is evident when comparing the effect on advective travel time and path length (compare Figure 5-12 and Figure 5-13 to Figure 5-24 and Figure 5-25). The hydraulic function of open boreholes from surface to repository depth in the repository area in Forsmark is also confirmed by the modelling study by Joyce et al. (2010). Their conclusion is that the groundwater flow pattern is affected and that the flow paths of the released particles change. Particles released at the deposition holes were attracted to all boreholes but one out of 33 simulated boreholes, and the results showed boreholes providing shortcuts between depth and the sheet joints. However, including an open borehole does not have a major effect on the performance measures.

One should also note the hydraulic effects of unsealed boreholes demonstrated above are for present day boundary conditions. During the temperate period, within the next 10,000 years, the Forsmark area, for example, is expected to be elevated approximately 40 m (SKB 2010). Therefore also the sea, which is the downstream boundary, will be displaced and the hydraulic gradient in the area will change. For the Forsmark site the present-day sea level boundary condition can be seen as a conservative (pessimistic) choice, since the effects of open boreholes, as easy path ways for groundwater flow between repository depth and surface, will decrease as the area undergoes a transition from a discharge area for deeper groundwater to more of a recharge area, similar to the present conditions at Laxemar. For the Laxemar site the trend will be similar: When the land-rise and shore-line displacement progresses (SKB 2010), the increased downward hydraulic gradient will increase the significance of open boreholes as paths for groundwater from surface to depth in the area.

6.2 Uncertainties and recommendations for further studies

In this study only one realization of the stochastic hydrogeological DFNs was applied in the simulations for each of the two sites. Introducing several realizations would allow investigation of the local variability, which especially has to be taken into account when comparing simulation results to measurements. The sensitivity of head and hydrochemical variables (as salinity and water types) to spatial heterogeneity due to different realizations of the DFN in models of the two sites are illustrated in SKB (2008, 2009a). The hydrochemical variables, such as salinity, were found to be quite sensitive to local spatial heterogeneity, whereas head was not so sensitive. It is recommended that multiple realizations are considered in future modelling of the hydraulic effects of open or poorly sealed boreholes. In order to be able to compare the simulation results to measurements from the boreholes in question it would also be favourable to introduce a base case DFN that is conditioned to the observed flowing anomalies in the boreholes.

Variable-density flow was not included in these models, nor the effects of heat flux from the repository. Ignoring salinity/density variations in space and time simplified the modelling approach considerably and allowed for use of a steady-state model. The assumption of constant density is in general conservative since an increasing groundwater density with depth tends to decrease vertical hydraulic gradients and vertical groundwater flow. Density and temperature effects may be important when assessing the long-term safety of borehole plugs.

In the simulations for both sites the zones of influence of the boreholes reach the no-flow bottom boundary of the model (Figure 5-2 and Figure 5-15). However, the noted effect of the boundary is smaller in the Laxemar model than in the Forsmark model. This difference may be due to both the different depths of the model domains (2.1 km compared to 1.2 km) and due to the differences in hydraulic conductivity at depth (cf. Sections 4.3.3 and 4.4.3). The effect of the boundary may diminish if salinity and density dependent flow is taken into account, but in future modelling one should extend the models deeper, further below the end of the boreholes.

A potential application of the models built in this study could be detailed studies of the design of borehole plugs in relation to hydrogeological structures. Then also the actual geometry of the planned repository could be implemented in the model.

7 Conclusions

- There is a difference in the hydraulic function of open investigation boreholes when comparing the Forsmark and Laxemar sites for the present-day hydraulic boundary conditions. In Forsmark open boreholes may acts as easy path ways for groundwater from repository depth to surface. In Laxemar, on the other hand, open boreholes may act as paths from surface to depth. This is because Forsmark is a discharge area for deeper groundwater whereas Laxemar is in part a recharge area.
- The open boreholes have a considerable influence on the hydraulic head in the surrounding bedrock at both sites. The influence of the plugged boreholes on head is insignificant.
- The open boreholes have a considerable influence on the groundwater turnover in the surrounding bedrock in the Forsmark model but not in the Laxemar model. In the Forsmark case the total flow through the borehole site rock volume is 17% above the natural flow with the boreholes open. The difference is explained by the much lower permeability at repository depth and by the larger magnitude of the vertical hydraulic gradient in Forsmark compared to Laxemar, which makes the influence of an open borehole larger in Forsmark. The influence of the plugged borehole on the total turnover is insignificant.
- The flow along the sections of the plugged boreholes that consist of degraded silica concrete (see section 2.1.6) is significantly above the natural flow in the surrounding rock due to the relatively high hydraulic conductivity of this material compared to that of the rock. However, the influence on the overall hydraulic head and flow field is insignificant. The bentonite sections have an important function to stop potential flow along the borehole towards the surface and to isolate transmissive structures that are intersected by the borehole. The positions of the bentonite sections in relation to transmissive structures are thus also important, especially for the Forsmark site where long concrete sections, with resulting continuous upward flow, are suggested.
- The open boreholes have a strong impact on solute transport in the surrounding bedrock at the Forsmark site but not at the Laxemar site. This is shown by the influence on the distributions of advective travel times and path lengths for particles. The influence of the plugged borehole (both reference plug design and a simplified design) is insignificant.

References

SKB's (Svensk Kärnbränslehantering AB) publications can be found at www.skb.se/publications.

Follin S, Johansson P-O, Hartley L, Jackson P, Roberts D, Marsic N, 2007. Hydrogeological conceptual model development and numerical modelling using CONNECTFLOW, Forsmark modelling stage 2.2. SKB R-07-49, Svensk Kärnbränslehantering AB.

Follin S, Hartley L, Jackson P, Roberts D, Marsic N, 2008. Hydrogeological conceptual model development and numerical modelling using CONNECTFLOW, Forsmark modelling stage 2.3. SKB R-08-23, Svensk Kärnbränslehantering AB.

Joyce S, Simpson T, Hartley L, Applegate D, Hoek J, Jackson P, Swan D, Marsic N, Follin S, 2010. Groundwater flow modelling of periods with temperate climate conditions – Forsmark. SKB R-09-20, Svensk Kärnbränslehantering AB.

Olofsson I, Simeonov A, Stephens M, Follin S, Nilsson A-C, Röshoff K, Lindberg U, Lanaro F, Fredriksson A, Persson L, 2007. Site descriptive modelling Forsmark, stage 2.2. A fracture domain concept as a basis for the statistical modelling of fractures and minor deformation zones, and interdisciplinary coordination. SKB R-07-15, Svensk Kärnbränslehantering AB.

Pusch R, Ramqvist G, Bockgård N, Ekman L, 2011. Sealing of investigation boreholes, Phase 4. Final report. SKB R-11-20, Svensk Kärnbränslehantering AB.

Rouhiainen P, Sokolnicki M, 2005. Oskarshamn site investigation. Difference flow logging of borehole KLX04. Subarea Laxemar. SKB P-05-68, Svensk Kärnbränslehantering AB.

Selroos J-O, Follin S, 2010. SR-Site groundwater flow modelling methodology, setup and results. SKB R-09-22, Svensk Kärnbränslehantering AB.

SKB, 2008. Site description of Forsmark at completion of the site investigation phase. SDM-Site Forsmark. SKB TR-08-05, Svensk Kärnbränslehantering AB.

SKB, 2009a. Site description of Laxemar at completion of the site investigation phase. SDM-Site Laxemar. SKB TR-09-01, Svensk Kärnbränslehantering AB.

SKB, 2009b. Underground design Forsmark. Layout D2. SKB R-08-116, Svensk Kärnbränslehantering AB.

SKB, 2009c. Underground design Laxemar. Layout D2. SKB R-09-16, Svensk Kärnbränslehantering AB.

SKB, 2010. Climate and climate-related issues for the safety assessment SR-Site. SKB TR-10-49, Svensk Kärnbränslehantering AB.

Sokolnicki M, 2007. Oskarshamn site investigation. Difference flow logging of borehole KLX10. Subarea Laxemar. SKB P-06-58, Svensk Kärnbränslehantering AB.

Sokolnicki M, Rouhiainen P, 2005. Oskarshamn site investigation. Difference flow logging in borehole KLX06. Subarea Laxemar. SKB P-05-74, Svensk Kärnbränslehantering AB.

Stephens M B, Fox A, La Pointe P, Simeonov A, Isaksson H, Hermanson J, Öhman J, 2007. Geology Forsmark. Site descriptive modelling Forsmark stage 2.2. SKB R-07-45, Svensk Kärnbränslehantering AB.

Svensson U, Ferry M, 2010. DarcyTools version 3.4. User's guide. SKB R-10-72, Svensk Kärnbränslehantering AB.

Svensson U, Follin S, 2010. Groundwater flow modelling of the excavation and operational phases – Forsmark. SKB R-09-19, Svensk Kärnbränslehantering AB.

Svensson U, Rhén I, 2010. Groundwater flow modelling of the excavation and operational phases – Laxemar. SKB R-09-23, Svensk Kärnbränslehantering AB.

Svensson U, Kuylenstierna H-O, Ferry M, 2010. DarcyTools version 3.4 – Concepts, methods and equations. SKB R-07-38, Svensk Kärnbränslehantering AB.

Vidstrand P, Rhén I, Zugec N, 2010. Groundwater flow modelling of periods with periglacial and glacial climate conditions – Laxemar. SKB R-09-25, Svensk Kärnbränslehantering AB.

Appendix 1

Compilation of input data to the DarcyTools groundwater flow models

Table A1-1. Input data to the Forsmark DarcyTools groundwater flow model.

Input data	File name and version/property value	Source
Geometry model domain outside FFM	domffm.dat 2008-03-16	SKBdoc
Geometry FFM1 bot	FFM01_06_below400.stl 2008-02-01	SKBdoc
Geometry FFM1 mid	FFM01_06_200_400.stl 2008-02-01	SKBdoc
Geometry FFM1 top	FFM01_06_above200.stl 2008-02-01	SKBdoc
Geometry FFM2	FFM02.stl 2008-02-01	SKBdoc
Geometry FFM3 bot	FFM03_05_below400.stl 2008-02-01	SKBdoc
Geometry FFM3 top	FFM03_05_above400.stl 2008-02-01	SKBdoc
Geometry FFM4 bot	FFM04_below400.stl 2008-02-01	SKBdoc
Geometry FFM4 top	FFM04_above400.stl 2008-02-01	SKBdoc
HCD (fracture file in format for deterministic fractures for DT)	HCD 2008-03-16	SKBdoc
Sheet joints (fracture file in format for deterministic fractures for DT)	HCDcage 2008-03-16	SKBdoc
Geometry watercourses	rivers.dat riversm2.dat riversp2.dat 2008-03-16	SKBdoc
Topography	top.dat 2008-03-16	SKBdoc
Geometry water divide	WD.dat 2008-03-16	SKBdoc
Geometry boreholes		Data delivery SICADA_08_123
Depth surface layer	20 m	Model delivery CFE 2008-06-19
Hydraulic conductivity in surface layer	$K_h = \max \begin{cases} 1\cdot10^{-7}\ \text{m/s} \\ 5\cdot10^{-3}\ 10^{-depth/3\ \text{m}}\ \text{m/s} \end{cases}$ $K_v = 1\cdot10^{-6}$ m/s	Model delivery CFE 2008-06-19
Hydraulic conductivity watercourses	$K_h = 2\cdot10^{-1}$ m/s	Model delivery CFE 2008-06-19
DFN parameters	See Appendix 2	
DFN fracture thickness	0.1 m	Model delivery CFE 2008-06-19
Hydraulic conductivity in rock outside FFM	depth< 200 m $K = 1\cdot10^{-7}$ m/s 200 m < depth < 400 m $K = 1\cdot10^{-8}$ m/s depth > 400 m $K = 3\cdot10^{-9}$ m/s	Selroos and Follin 2010, Table 2-6
Hydraulic conductivity in rock, minimum	$3\cdot10^{-9}$ m/s	Model delivery CFE 2008-06-19
Kinematic porosity in surface layer	$\theta = \max \begin{cases} 1\cdot10^{-3} \\ 5\cdot10^{-2}\ 10^{-\text{depth}/20\ m} \end{cases}$	Model delivery CFE 2008-06-19
Kinematic porosity in rock	$\theta = \max \begin{cases} 1\cdot10^{-5} \\ frevol/vol \end{cases}$	Model delivery CFE 2008-06-19
Location of borehole plugs		Pusch et al. 2011
Hydraulic conductivity of borehole plug	Silica concrete: $K = 1\cdot10^{-6}$ m/s Bentonite: $K = 1\cdot10^{-8}$ m/s	Pusch et al. 2011

SKBdoc. Model: Numerical groundwater flow modelling of the Forsmark and Laxemar site.zip, Version 1.0 Approved 2012-06-05, Modeller: N. Bockgård. ID:1345675 (access might be given on request).

Table A1-2. Input data to the Laxemar DarcyTools groundwater flow model.

Input data	File name and version/property value	Source
HRD domains	FD_LX_LOC_V23b-c_HydroVolume_2_stl.zip	Trac (SDM)
HCD	090423_ls_Reg_Loc_Disks_Dol_100_Cond_24_dt.zip	Trac (HCD)
DFN	090507_ls_md2_sets1_64_asc.zip	Trac (fractures)
Geometry watercourses	DTStreams_05km2_from_umeu_sm_hoj_4530.zip	Trac (CFE)
Topography	sdeadm_umeu_sm_hoj_4530.asc	Data delivery GIS_09_31
Geometry water divide	Outer_boundary_trim5.stl	Trac (SDM)
Geometry boreholes		Data delivery SICADA_08_123
Depth surface layer	20 m	Model delivery CFE 2009-05-13
Hydraulic conductivity in surface layer	$K_h = \max \begin{cases} 1\cdot10^{-7}\ \text{m/s} \\ 5\cdot10^{-3}\ 10^{-depth/3\ \text{m}}\ \text{m/s} \end{cases}$ $K_v = 5\cdot10^{-6}$ m/s	Model delivery CFE 2009-05-13
Hydraulic conductivity watercourses	K_h function of easting coordinate: $K_h = K_v\ (0.1+0.9\ X/21000\ \text{m})$ $K_v = 2\cdot10^{-1}$ m/s	Model delivery CFE 2009-05-13
DFN parameters for detailed DFN around borehole	See Appendix 3	
DFN fracture thickness	0.1 m	Model delivery CFE 2009-05-13
Hydraulic conductivity in rock, minimum	$1\cdot10^{-10}$ m/s	Model delivery CFE 2009-05-13
Kinematic porosity in surface layer	$\theta = \max \begin{cases} 1\cdot10^{-3} \\ 5\cdot10^{-2}\ 10^{-\text{depth}/20\ m} \end{cases}$	Model delivery CFE 2009-05-13
Kinematic porosity in rock	$\theta = \max \begin{cases} 5\cdot10^{-5} \\ frevol/vol \end{cases}$	Model delivery CFE 2009-05-13
Location of borehole plugs		Pusch et al. 2011
Hydraulic conductivity of borehole plug	Silica concrete: $K = 1\cdot10^{-6}$ m/s Bentonite: $K = 1\cdot10^{-8}$ m/s	Pusch et al. 2011

Trac (CFE) Path: SR-Site Data Storage/CFE/Open repository Laxemar.
Trac (SDM) Path: SR-Site Data Storage/SDM_GWF_Domain_to_stl-format/Laxemar.
Trac (HCD) Path: SR-Site Data Storage/SERCO/hcd/Laxemar.
Trac (fractures) Path: SR-Site Data Storage/SERCO/Laxemar/fractures.

Appendix 2

Parameters of the Forsmark hydrogeological DFN model

The applied hydrogeological DFN model was from a preliminary version of the Forsmark 2.2 model (Follin et al. 2007), and hence the parameter values used here do not correspond exactly to the final version. The parameter values were compiled for a preliminary version (dated June 2008) of the DarcyTools model reported in (Svensson and Follin 2010) and are given in Tables A2-1 to A2-6. The meaning of the DarcyTools DFN parameters are defined in Svensson and Ferry (2010).

Table A2-1. DFN parameters for fracture domains FFM01 and FFM06 above –200 m RHB 70.

Parameter	Set 1 (NS)	Set 2 (NE)	Set 3 (NW)	Set 4 (EW)	Set 5 (HZ)
Reference length, l_{ref} (m)	1.0	1.0	1.0	1.0	1.0
Cut-off length, r_0 (m)	0.038	0.038	0.038	0.038	0.038
Power law exponent, p (–)	–2.55	–2.75	–3.10	–3.10	–2.42
DT intensity (m^{-3})	0.01222	0.03880	0.00571	0.00560	0.08370
P_{32} (m^{-1})	0.094	0.366	0,101	0,099	0,619
Orientation distribution vector, λ (–)	(–16.500, 6.667, –0.311)	(–7.990, 11.840, –0.499)	(11.110, 6.410, –1.348)	(3.620, 13.510, –0.489)	(0.0924, 1.056, –15.160)
Trend (°)	292	326	60	15	5
Plunge (°)	1	2	6	2	86
Fisher conc., κ (–)	17.8	14.3	12.9	14.0	15.2

Table A2-2. DFN parameters for fracture domains FFM01 and FFM06 below –200 m and above –400 m RHB 70.

Parameter	Set 1 (NS)	Set 2 (NE)	Set 3 (NW)	Set 4 (EW)	Set 5 (HZ)
Reference length, l_{ref} (m)	1.0	1.0	1.0	1.0	1.0
Cut-off length, r_0 (m)	0.038	0.038	0.038	0.038	0.038
Power law exponent, p (–)	–2.55	–2.75	–3.10	–3.10	–2.42
DT intensity (m^{-3})	0.0286	0.0428	0.00763	0.00594	0.0448
P_{32} (m^{-1})	0.220	0.404	0.135	0.105	0.331
Orientation distribution vector, λ (–)	(–16.500, 6.667, –0.310)	(–7.990, 11.850, –0.499)	(11.110, 6.410, –1.348)	(3.620, 13.510, –0.489)	(0.0920, 1.056, –15.160)
Trend (°)	292	326	60	15	5
Plunge (°)	1	2	6	2	86
Fisher conc., κ (–)	17.8	14.3	12.9	14.0	15.2

Table A2-3. DFN parameters for fracture domains FFM01 and FFM06 below –400 m RHB 70.

Parameter	Set 1 (NS)	Set 2 (NE)	Set 3 (NW)	Set 4 (EW)	Set 5 (HZ)
Reference length, l_{ref} (m)	1.0	1.0	1.0	1.0	1.0
Cut-off length, r_0 (m)	0.038	0.038	0.038	0.038	0.038
Power law exponent, p (–)	–2.55	–2.75	–3.10	–3.10	–2.42
DT intensity (m^{-3})	0.0152	0.0191	0.00566	0.00317	0.0214
P_{32} (m^{-1})	0.117	0.180	0.100	0.056	0.158
Orientation distribution vector, λ (–)	(–16.500, 6.667, –0.310)	(–7.990, 11.850, –0.499)	(11.110, 6.410, –1.348)	(3.620, 13.510, –0.489)	(0.0920, 1.056, –15.160)
Trend (°)	292	326	60	15	5
Plunge (°)	1	2	6	2	86
Fisher conc., κ (–)	17.8	14.3	12.9	14.0	15.2

Table A2-4. DFN parameters for fracture domain FFM02.

Parameter	Set 1 (NS)	Set 2 (NE)	Set 3 (NW)	Set 4 (EW)	Set 5 (HZ)
Reference length, l_{ref} (m)	1.0	1.0	1.0	1.0	1.0
Cut-off length, r_0 (m)	0.038	0.038	0.038	0.038	0.038
Power law exponent, p (–)	–2.75	–2.62	–3.20	–3.40	–2.58
DT intensity (m^{-3})	0.0493	0.0620	0.0154	0.00370	0.195
P_{32} (m^{-1})	0.380	0.585	0.272	0.065	1.44
Orientation distribution vector, λ (–)	(–16.500, 6.667, –0.310)	(–7.990, 11.850, –0.499)	(11.110, 6.410, –1.348)	(3.620, 13.510, –0.489)	(0.0920, 1.056, –15.160)
Trend (°)	292	326	60	15	5
Plunge (°)	1	2	6	2	86
Fisher conc., κ (–)	17.8	14.3	12.9	14.0	15.2

Table A2-5. DFN parameters for fracture domains FFM03, FFM04, and FFM05 above –400 m RHB 70.

Parameter	Set 1 (NS)	Set 2 (NE)	Set 3 (NW)	Set 4 (EW)	Set 5 (HZ)
Reference length, l_{ref} (m)	1.0	1.0	1.0	1.0	1.0
Cut-off length, r_0 (m)	0.038	0.038	0.038	0.038	0.038
Power law exponent, p (–)	–2.60	–2.50	–2.55	–2.40	–2.55
DT intensity (m^{-3})	0.0088	0.0362	0.0318	0.0188	0.0495
P_{32} (m^{-1})	0.068	0.341	0.562	0.332	0.366
Orientation distribution vector, λ (–)	(–16.500, 6.667, –0.310)	(–7.990, 11.850, –0.499)	(11.110, 6.410, –1.348)	(3.620, 13.510, –0.489)	(0.0920, 1.056, –15.160)
Trend (°)	292	326	60	15	5
Plunge (°)	1	2	6	2	86
Fisher conc., κ (–)	17.8	14.3	12.9	14.0	15.2

Table A2-6. DFN parameters for fracture domains FFM03, FFM04, and FFM05 below –400 m RHB 70.

Parameter	Set 1 (NS)	Set 2 (NE)	Set 3 (NW)	Set 4 (EW)	Set 5 (HZ)
Reference length, l_{ref} (m)	1.0	1.0	1.0	1.0	1.0
Cut-off length, r_0 (m)	0.038	0.038	0.038	0.038	0.038
Power law exponent, p (–)	–2.60	–2.50	–2.55	–2.40	–2.55
DT intensity (m^{-3})	0.0084	0.0398	0.0106	0.00761	0.0328
P_{32} (m^{-1})	0.065	0.376	0.187	0.135	0.243
Orientation distribution vector, λ (–)	(–16.500, 6.667, –0.310)	(–7.990, 11.850, –0.499)	(11.110, 6.410, –1.348)	(3.620, 13.510, –0.489)	(0.0920, 1.056, –15.160)
Trend (°)	292	326	60	15	5
Plunge (°)	1	2	6	2	86
Fisher conc., κ (–)	17.8	14.3	12.9	14.0	15.2

Appendix 3

Parameters of the Laxemar hydrogeological DFN model

The applied hydrogeological DFN model was the model described in SKB (2009a), and the so-called hydrogeological DFN model base case realization covering the whole model domain was imported into DarcyTools. Thus only the detailed DFN around borehole KLX06 was generated within DarcyTools. The parameter values for the DarcyTools setup were those compiled by Vidstrand et al. (2010) and are given in Tables A3-1 to A3-4. The meaning of the DarcyTools DFN parameters are defined in Svensson and Ferry (2010).

Table A3-1. DFN parameters for hydraulic rock domains HRD_N and HRD_A above –150 m RHB 70.

Parameter	Set 1 (ENE)	Set 2 (WNW)	Set 3 (NS)	Set 4 (sub-H)
Reference length, l_{ref} (m)	1.0	1.0	1.0	1.0
Cut-off length,r_0 (m)	0.038	0.038	0.038	0.038
Power law exponent, p (–)	–2.50	–2.30	–2.50	–2.70
DT intensity (m^{-3})	0.05364	0.13016	0.06018	0.14315
P_{32} (m^{-1})	0.41	0.92	0.46	1.35
Orientation distribution vector, λ (–)	(–4.82996, 15.04355, –0.05515)	(–7.25299, –12.66444, –0.40766)	–10.27471, 0.23317, –0.68262)	–1.60737, –0.96963, –12.56050)
Trend (°)	342.2	209.8	271.3	238.9
Plunge (°)	0.2	1.6	3.8	81.5
Fisher conc., κ (–)	15.8	14.6	10.3	12.7

Table A3-2. DFN parameters for hydraulic rock domains HRD_N and HRD_A below –150 m and above –400 m RHB 70.

Parameter	Set 1 (ENE)	Set 2 (WNW)	Set 3 (NS)	Set 4 (sub-H)
Reference length, l_{ref} (m)	1.0	1.0	1.0	1.0
Cut-off length, r_0 (m)	0.038	0.038	0.038	0.038
Power law exponent, p (–)	–2.80	–2.40	–2.80	–2.75
DT intensity (m^{-3})	0.03791	0.07503	0.03606	0.12702
P_{32} (m^{-1})	0.41	0.54	0.39	1.28
Orientation distribution vector, λ (–)	(–4.82996, 15.04355, -0.05515)	(–7.25299, –12.66444, –0.40766)	–10.27471, 0.23317, –0.68262)	–1.60737, –0.96963, –12.56050)
Trend (°)	342.2	209.8	271.3	238.9
Plunge (°)	0.2	1.6	3.8	81.5
Fisher conc., κ (–)	15.8	14.6	10.3	12.7

Table A3-3. DFN parameters for hydraulic rock domains HRD_N and HRD_A below –400 m and above –650 m RHB 70.

Parameter	Set 1 (ENE)	Set 2 (WNW)	Set 3 (NS)	Set 4 (sub-H)
Reference length, l_{ref} (m)	1.0	1.0	1.0	1.0
Cut-off length, r_0 (m)	0.038	0.038	0.038	0.038
Power law exponent, p (–)	–2.60	–2.40	–2.60	–2.70
DT intensity (m^{-3})	0.03101	0.05002	0.02982	0.04348
P_{32} (m^{-1})	0.26	0.36	0.25	0.41
Orientation distribution vector, λ (–)	(–4.82996, 15.04355, -0.05515)	(–7.25299, –12.66444, –0.40766)	–10.27471, 0.23317, –0.68262)	–1.60737, –0.96963, –12.56050)
Trend (°)	342.2	209.8	271.3	238.9
Plunge (°)	0.2	1.6	3.8	81.5
Fisher conc., κ (–)	15.8	14.6	10.3	12.7

Table A3-4. DFN parameters for hydraulic rock domains HRD_N and HRD_A below –650 m RHB 70.

Parameter	Set 1 (ENE)	Set 2 (WNW)	Set 3 (NS)	Set 4 (sub-H)
Reference length, l_{ref} (m)	1.0	1.0	1.0	1.0
Cut-off length, r_0 (m)	0.038	0.038	0.038	0.038
Power law exponent, p (–)	–2.90	–2.80	–2.95	–2.95
DT intensity (m^{-3})	0.02779	0.04161	0.00586	0.00513
P_{32} (m^{-1})	0.35	0.45	0.08	0.07
Orientation distribution vector, λ (–)	(–4.82996, 15.04355, -0.05515)	(–7.25299, –12.66444, –0.40766)	–10.27471, 0.23317, –0.68262)	–1.60737, –0.96963, –12.56050)
Trend (°)	342.2	209.8	271.3	238.9
Plunge (°)	0.2	1.6	3.8	81.5
Fisher conc., κ (–)	15.8	14.6	10.3	12.7